*Acta Geologica Polonica*, Vol. 76 (2026), No. 2, e76
DOI: 10.24425/agp.2026.158190

# Morphotectonic and structural signatures of the Savrun Fault: implications for its Neogene evolution (SE Turkey)

AHMET CAN AKINCI[1], ULVİ CAN ÜNLÜGENÇ[1], HAKAN GÜNEYLİ[1], ERHAN ALTUNEL[2], ALİ GÖKHAN ÖÇGÜN[1] and İBRAHİM ADLIĞ[1]

[1] *Çukurova University, Engineering Faculty, Geological Engineering Department, Adana/Türkiye; e-mails: acakinci@cu.edu.tr, ulvican@cu.edu.tr hguneyli@cu.edu.tr gokalit@gmail.com, ibrahimadlig288@gmail.com*
[2] *Eskişehir Osmangazi University, Engineering Faculty, Geological Engineering Department, Eskişehir/Türkiye; e-mail: ealtunel@ogu.edu.tr*

ABSTRACT:

Akıncı, A.C., Ünlügenç, U.C., Güneyli, H., Altunel, E., Öçgün, A.G. and Adlığ, İ. 2026. Morphotectonic and structural signatures of the Savrun Fault: implications for Its Neogene evolution (SE Turkey). *Acta Geologica Polonica*, **76** (2), e76.

The destructive earthquakes of February 6, 2023 in southern Turkey renewed scientific interest in neighboring fault systems whose late-stage tectonic histories remain poorly constrained. One such structure is the Savrun Fault, located northeast of Adana and southwest of the Sürgü-Çardak Fault. This study investigates the tectonic character and Neogene to Quaternary evolution of the Savrun Fault through an integrated approach that combines field observations, lithostratigraphic relationships, morphotectonic indices and GIS-based remote-sensing analyses. The fault extends from Kozan toward Göksun and exhibits well-developed structural elements, including fault planes, fracture systems and associated deformation within Lower to Middle Miocene sedimentary units. In contrast, overlying Quaternary colluvial and alluvial deposits show no evidence of displacement or disruption. Morphotectonic indices (S*mf*, SL, HI, A*f*, V*f*) reveal localized landscape modification, yet the undisturbed nature of young fluvial and alluvial units indicates that the fault has not experienced documented reactivation during the Quaternary. Despite its close spatial relationship to the seismically active Sürgü-Çardak Fault, the Savrun Fault lacks geomorphic or stratigraphic indicators of late-stage slip. Its southern segment, particularly near the Bağdaş Plateau, is interpreted as a transpressional zone that likely ceased motion during the Middle to Late Miocene. These combined observations suggest that, although structurally prominent, the Savrun Fault plays no measurable role in present-day deformation. The refined tectonic interpretation presented here contributes to a clearer understanding of fault architecture and Neogene landscape evolution in the central Amanos-Göksun region.

**Key words:** Savrun Fault; Southeast Anatolia; Neogene tectonics; Morphotectonic analysis; Structural geology.

## INTRODUCTION

The Savrun Fault (SF), located along the northeastern margin of the Adana Basin in southeastern Turkey, occupies a tectonically sensitive position between the Central Tauride units and the Miocene–Quaternary basin infill (Text-fig. 1). Although previously regarded as a morphotectonic lineament with uncertain late-stage deformation (Pampal 1983; Emre *et al.* 2013; Gürboğa 2025), the destructive earthquakes of 6 February 2023 (Mw 7.8 and Mw 7.6) (AFAD 2023, 2024; KRDAE 2023) have renewed

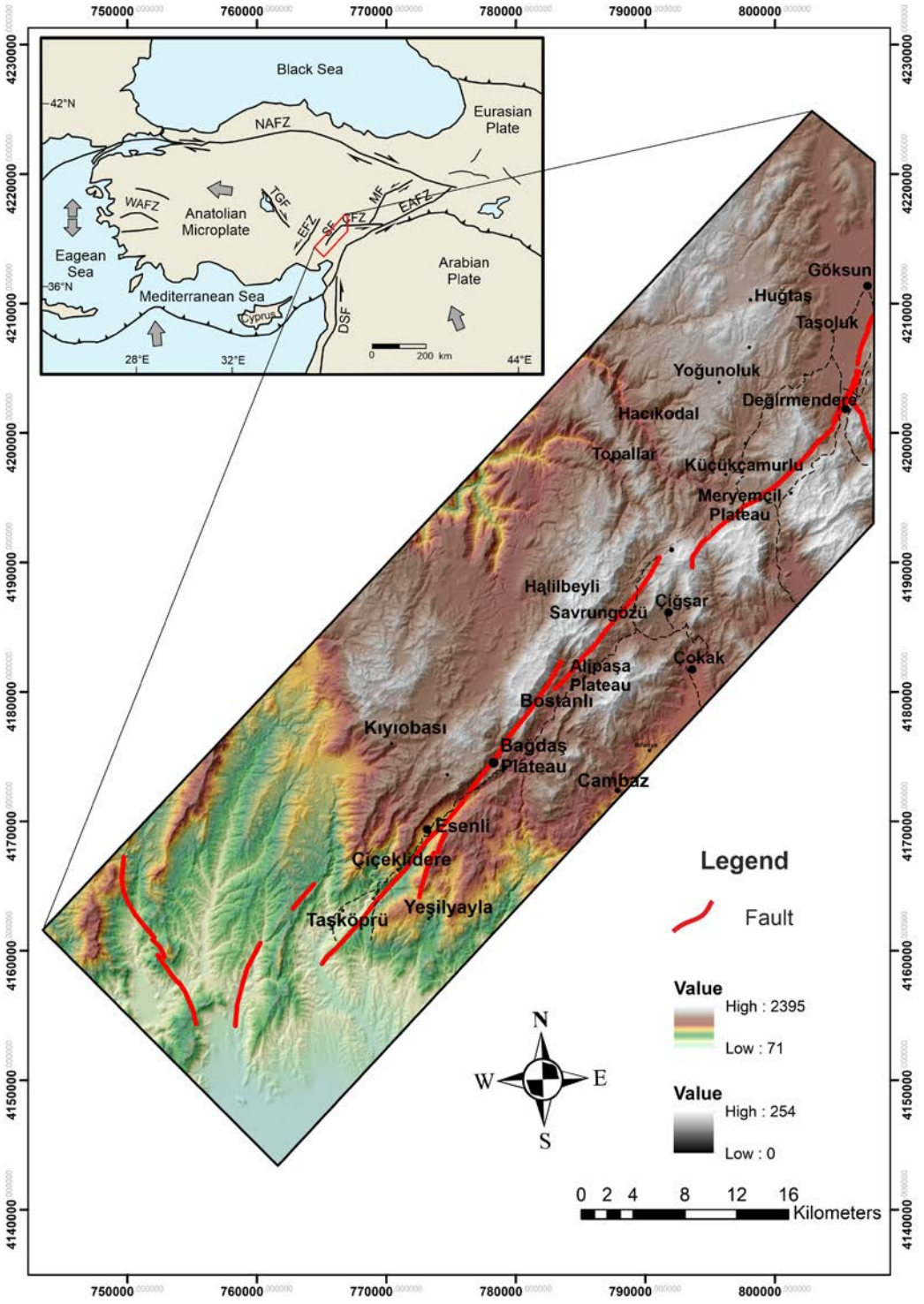


Fig. 1. DEM-based shaded-relief topographic map of the Savrun Fault Zone showing the full extent of the Savrun Fault and surrounding geomorphology. The main fault trace and other active faults are compiled from the Active Fault Map of Turkey (MTA, 2023). Major settlements and geographic features, including Kozan and Göksun, are indicated to provide spatial context. Elevation and hillshade are derived from high-resolution ALOS 12.5 m DEM data. The inset map illustrates the regional neotectonic framework of Anatolia and adjacent regions, highlighting major fault systems and plate boundaries, with the study area outlined in red. Fault abbreviations: NAFZ: North Anatolian Fault Zone; EAFZ: East Anatolian Fault Zone; ÇFZ: Sürgü-Çardak Fault Zone; SF: Savrun Fault; EFZ: Ecemiş Fault Zone; TGF: Tuzgölü Fault; WAFZ: Western Anatolian Fault Zone.

scientific attention on the broader fault architecture of the region.

In the weeks and months following the 2023 mainshocks, thousands of aftershocks were recorded across southeastern Anatolia, some occurring in the vicinity of the Savrun Fault (AFAD 2023). This widespread seismicity highlighted the need to better understand the structural configuration and Neogene–Quaternary evolution of neighboring faults.

The structural relationship between the Savrun and Çardak faults is of particular interest. The Savrun Fault emerges immediately south of the point where the surface rupture of the Çardak Fault, which hosted the afternoon Mw 7.6 Elbistan earthquake of the February 6, 2023 doublet, terminates near the village of Aslanbeyçiftliği, then bends sharply southward and extends toward the northern margin of the Miocene Adana Basin along a SW-NE trend (Ünlügenç 1993) (Text-fig. 1). This abrupt change in orientation raises the possibility of past kinematic linkage between the two systems and suggests that the Savrun Fault may once have accommodated regional strain transfer. However, its present-day tectonic activity remains poorly constrained. The ~85 km long Çardak Fault extends between Nurhak and Göksun with a broadly east-west, concave geometry. Near Ericek, the fault exhibits a right-stepping arrangement across a ~500-m-wide relay zone before curving southwestward and linking with the NE-SW-trending Savrun Fault (Koç 2005; Sunkar *et al.* 2008; Koç and Kaymakçı 2013; Balkaya *et al*. 2021). Although several studies, most notably Koç (2005), Sunkar *et al.* (2008), and Koç and Kaymakçı (2013), interpret the combined Sürgü-Çardak Fault Zone as a dominantly dextral strike-slip system with local reverse components, broader regional assessments emphasize a predominantly sinistral character in line with the kinematics of the East Anatolian Fault Zone. The 2023 Elbistan earthquake (Mw 7.6), however, produced ~4 m of left-lateral displacement along the Çardak segment, clearly demonstrating both its active seismogenic behavior and the inherently complex, multi-component slip kinematics of the system (Akıncı and Ünlügenç 2023).

The Savrun Fault is shown in national-scale compilations of the Turkish Active Fault Map (Text-fig. 1; Emre *et al.* 2013, 2018); however, its recent activity and neotectonic significance have been interpreted differently in the literature. To address this issue, we integrate field-based geological and structural observations with geomorphic analysis using high-resolution topography and satellite imagery. Quantitative morphometric indices (e.g., SL, S*mf*, V*f*, A*f*, HI) are employed to evaluate landscape response to tectonics, while reconnaissance-scale paleoseismic investigations provide additional constraints on possible Quaternary deformation (Bull and McFadden 1977; Keller and Pinter 2002; Burbank and Anderson 2012). This multidisciplinary approach allows us to distinguish inherited morphological features from indicators of active faulting.

Previous studies have described fault-related landforms such as linear valleys, deflected streams, and fault breccias within Miocene units (Ünlügenç *et al.* 2011; Ünlügenç and Akıncı 2019). However, evidence of deformation in younger Quaternary deposits, including alluvial fans and river terraces, remains absent or inconclusive. This discrepancy has generated uncertainty over whether the Savrun Fault has been tectonically active during the Holocene. Clarifying this issue is critical for refining seismic hazard assessments in a region recently impacted by major earthquakes.

This study provides one of the first multidisciplinary evaluations of the tectonic activity of a structurally significant fault situated within a zone of recent large earthquakes and ongoing public concern. By differentiating inherited morphologic signals from indicators of active deformation, the results contribute to improved seismic hazard assessments and emphasize the importance of reevaluating "silent" faults in post-earthquake risk mapping efforts.

In this study, the terms inactive, quiescent, nonreactivated, and lacking neotectonic activity are used within a clearly defined temporal and methodological framework and are not intended as interchangeable expressions. Here, the neotectonic period is considered to encompass Late Pleistocene to Holocene deformation (approximately post-MIS 5), consistent with regional neotectonic definitions proposed for southern Anatolia and Turkey (Bozkurt 2001; Şengör *et al*. 2005). Accordingly, the term "inactive" refers specifically to the absence of demonstrable Late Pleistocene–Holocene surface deformation, rather than to the complete cessation of fault motion since the Miocene. In this context, inactivity denotes the lack of observable surface rupture, measurable displacement, or geomorphic expression within Quaternary deposits at the scale and resolution of the applied geological, geomorphic, and remote sensing datasets (Keller and Pinter 2002). All statements regarding fault activity or inactivity should therefore be understood as constrained by this temporal window and by the detection limits of the methods employed.

## GEOLOGICAL AND TECTONIC SETTING OF THE REGION

While paleoseismological investigations commonly emphasize fault morphology and recent tectonic activity, evaluation of the Savrun Fault Zone (SFZ) requires consideration of its broader geological framework. The SFZ lies within a structurally complex region comprising Paleozoic to Neogene lithological units that record multiple tectonic phases. Consequently, interpretation of fault geometry, kinematics, and possible activity must be grounded in the regional stratigraphic and structural architecture (Westaway 2003, 2004; Koç and Kaymakçı 2013; Ünlügenç and Akıncı 2018). Previous studies have provided only limited constraints on the detailed structural evolution of the fault system. The SFZ and its surroundings, located within the Eastern Taurus Mountains, evolved under a highly complex tectonic regime within the broader geodynamic framework of southeastern Turkey (Özgül *et al.* 1972; Özgül 1976; Özdoğan and Şahbaz 1993; Özgül and Kozlu 1993, 2002). This complexity reflects the superposition of tectonostratigraphic units of different ages formed during successive deformation phases. Regional evolution is primarily linked to the progressive closure of the Southern Neotethys from the Late Cretaceous to the Miocene (Şengör and Yılmaz 1981; Kelling *et al.* 1987, 2001; Yılmaz *et al.* 1985; Karig and Kozlu 1990; Robertson 1998, 2000; Robertson *et al.* 2004; Akıncı *et al.* 2016; Nurlu *et al.* 2016; Hozatlıoğlu *et al.* 2020; Darbaş *et al.* 2021; Akıncı and Ünlügenç 2021; Ünlügenç and Akıncı 2024). According to widely accepted models, convergence between the Arabian

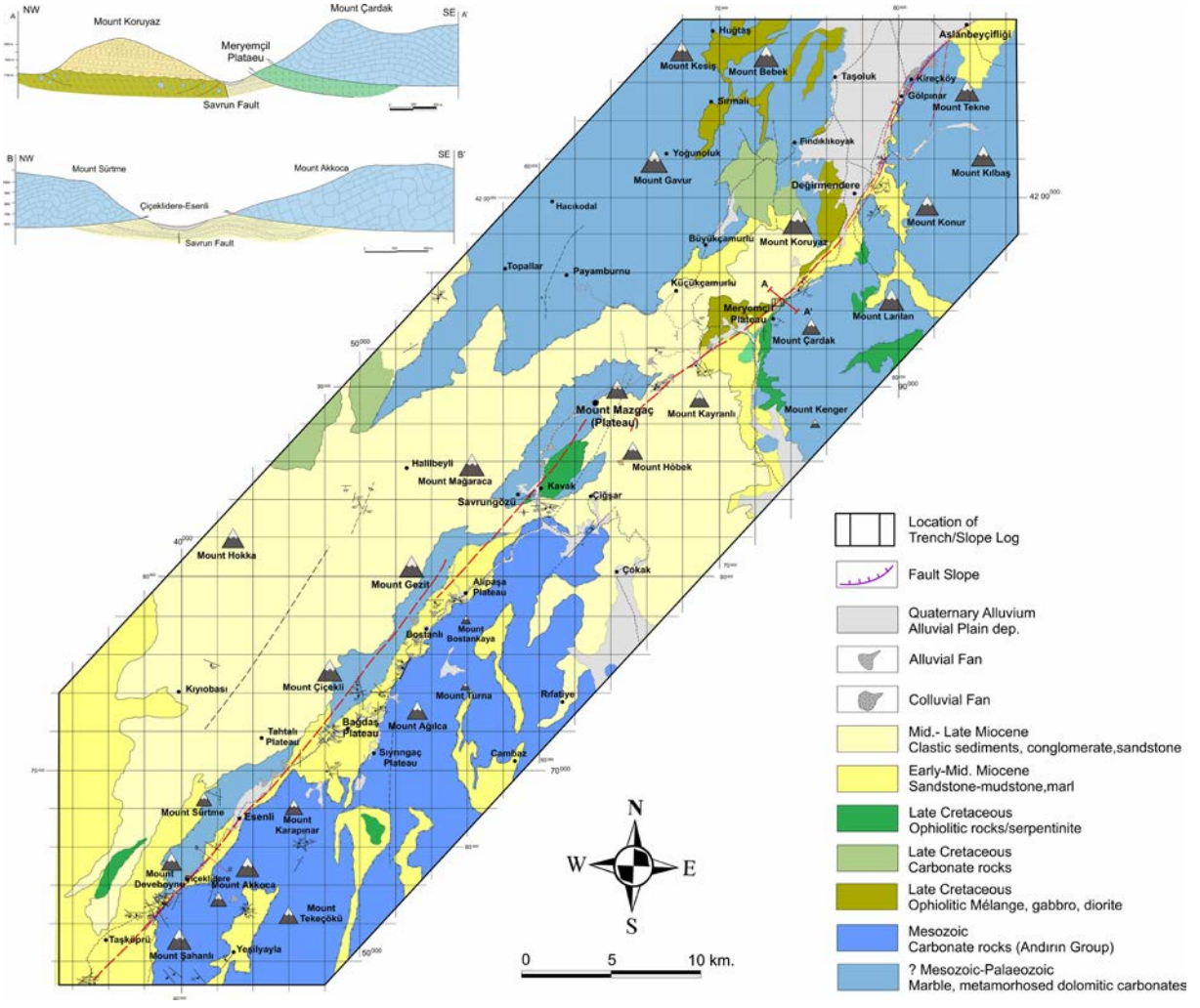


Fig. 2. Geological map of the Savrun Fault and its surrounding region, adapted from Akbaş *et al.* (2011). The map illustrates major mountain systems, key settlements, and detailed geological cross-sections, providing an integrated view of the structural and stratigraphic framework of the area.

and Anatolian plates resulted in progressive subduction and continental collision, leading to closure of the Neotethyan domain (Hall 1976; Rotstein and Ben-Avraham 1985; Aktaş and Robertson 1990; Ünlügenç 1993), although the precise timing and mechanisms remain debated.

To the north, compressional interactions between the Anatolian Plate, characterized by Paleozoic–Mesozoic carbonate and clastic sequences, and the Arabian Plate resulted in the emplacement of ophiolitic rocks and mélange complexes during the Late Cretaceous (Şengör and Yılmaz 1981; Kelling *et al.* 1987, 2001; Yılmaz *et al.* 1985; Karig and Kozlu 1990; Yılmaz and Gürer 1996; Robertson *et al.* 2004). Continued compression led to the progressive closure of foreland basins and culminated in continental collision by the Miocene. Sedimentary units deposited during this interval were subsequently deformed under compressional tectonics and were locally overprinted by older Paleozoic and Mesozoic structural fabrics. These processes collectively produced the structurally complex architecture that characterizes the Eastern Taurus region.

The Savrun Fault, first identified by Pampal (1983), originates along the southern slopes of the Eastern Taurus, forms the northern boundary of the Çukurova Plain, and extends northeastward through the Kozan region toward the Göksun Plain (Text-fig. 1). Along its trace, the fault follows a linear morphostructural corridor that separates two major geological assemblages, the Andırın and Gezitdağı units. In the eastern sector, the Andırın Unit comprises both autochthonous and allochthonous sequences (Blumenthal 1952; Tutkun 1989; Ünlügenç 1993; Güneyli 1995; Güneyli *et al.* 1996; Bozkaya 1998; Usta *et al.* 2004, 2013; Akıncı and Ünlügenç 2021), whereas the western sector is dominated by autochthonous successions of the Gezitdağı Unit (Ayhan 1983; Bedi *et al.* 2006; Bedi and Usta 2006) (Text-fig. 2).

The Gezitdağı Unit constitutes the regional basement of the study area and is composed predominantly of Permian carbonates, dolomitic limestones, and locally metamorphosed rocks. Sedimentation within this western succession was limited during much of the Mesozoic, although remnants of Late Cretaceous ophiolitic complexes related to the consumption and obduction of oceanic lithosphere are locally preserved. These basement and Upper Cretaceous units are unconformably overlain by Paleocene–Eocene carbonate-dominated Paleogene sequences and subsequently by widespread Miocene clastic successions, including the Early–Middle Miocene Savrun Formation and the Langhian Gezitdağı Formation (Text-fig. 3).

The Miocene units form extensive valley-fill and basin-margin deposits along the Savrun Fault corridor and record syn- to post-tectonic sedimentation associated with regional Neogene deformation. In the eastern sector, these clastic successions rest directly on Mesozoic units along major tectonic contacts, reflecting significant structural reorganization during the Early–Middle Miocene. This stratigraphic architecture, characterized by unconformities, tectonic contacts, and contrasting lithologies, provides an important geological framework for evaluating the structural evolution and surface expression of the Savrun Fault.

## METHODOLOGY

This study employed an integrated methodological framework combining field-based structural analysis, morphometric indices, and GIS-supported spatial evaluations to assess the neotectonic activity and structural characteristics of the Savrun Fault in the northeastern Adana Basin. The methodological workflow is outlined below.

### Field-based structural and paleoseismological reconnaissance

Detailed geological fieldwork was conducted to map lithostratigraphic boundaries, identify fault traces, and measure fault planes using a Brunton-type compass. Particular attention was given to recording slickenside lineations, fault plane orientations, and associated deformation structures in various lithologies, ranging in age from Paleozoic to Quaternary. Structural data were analyzed using stereonet projection and kinematic interpretation techniques (e.g., Linked Bingham analysis) to determine the dominant fault regimes. Stereographic projections and kinematic analyses were generated using FaultKin 8.3 software. The number of measurements (n) for each stratigraphic unit is specified within the corresponding subsection of the Results. Raw structural data are available from the corresponding author upon reasonable request and subject to the data-sharing agreement with the funding institution. In regions where surface exposures allowed, fault zones were examined for paleoseismological indicators such as fault scarps, colluvial wedges, and displaced strata (e.g., El Hamdouni *et al.* 2008; Dehbozorgi *et al.* 2010; Burbank and Anderson 2013). Although no trenching was conducted due to the lack of clear fault traces within the Quaternary deposits, several key slope exposures were studied in detail through sys-

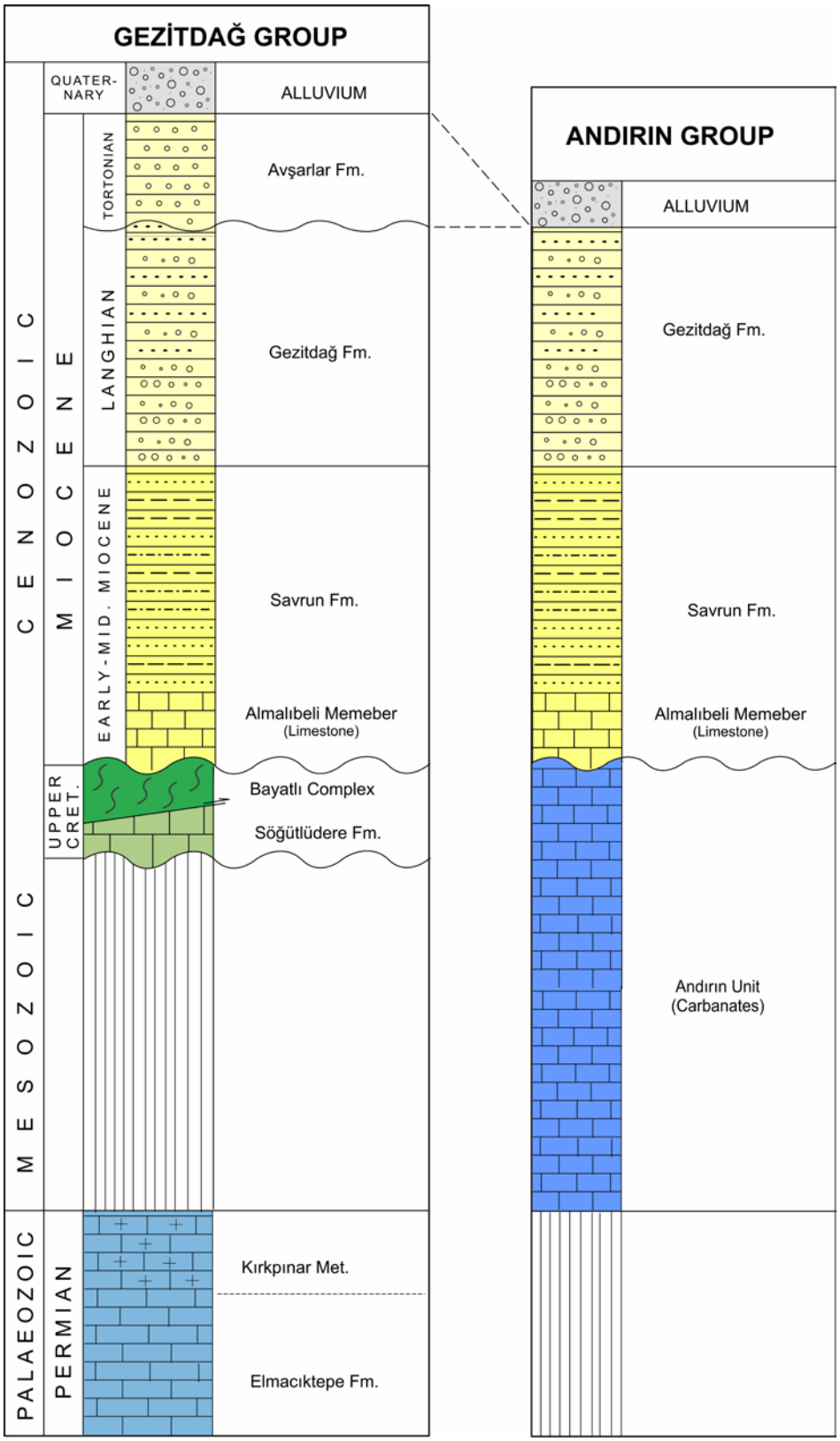


Fig. 3. A stratigraphic columnar section showing the relationships of the main geological units (Gezitdağ and Andırın Formations) around the Savrun Fault (Pampal, 1983; This study).

tematic gridding and logging. These observations are therefore interpreted as paleoseismological reconnaissance rather than trench-based or chronologically constrained paleoseismological investigations.

In addition, high-resolution drone imagery was systematically acquired using a DJI Mini 4 Pro unmanned aerial vehicle (UAV). Flights were conducted at variable altitudes up to approximately 400–500 m above ground level, yielding ground sampling distances of ~10–20 cm/pixel with ≥80% image overlap. These photographs were used directly for visual interpretation and integrated with field observations within the GIS environment. The aerial imagery provided a synoptic view of fault corridors, linear valleys, and surface deformation patterns, enhancing the identification and mapping of fault traces and paleoseismological features that are otherwise difficult to capture solely from ground-based measurements.

## Morphometric analysis and tectonic geomorphology

To assess potential tectonic activity, a range of morphometric indices (e.g.: Goudie 2004; Selim *et al.* 2013) were calculated based on high-resolution Digital Elevation Models (DEMs) with a spatial resolution of 12.5 meters and a vertical accuracy of ~±12.7 m (derived from ALOS PALSAR data). These indices include:

- Hypsometric Integral (HI) and hypsometric curve analysis to evaluate stages of landscape evolution (Strahler 1952; Pike and Wilson 1971; Burbank and Anderson 2012);
- Stream Length-Gradient Index (SL) to identify anomalies in longitudinal river profiles (Hack 1973);
- Valley Floor Width to Valley Height Ratio (V*f*) to assess tectonic uplift and valley morphology (Hack 1973; Bull 1977);
- Mountain Front Sinuosity (S*mf*) to evaluate the balance between erosion and tectonic uplift (Bull and McFadden 1977; Keller and Pinter 1996); and
- Basin Asymmetry Factor (A*f*) to characterize drainage basin tilting (Hare and Gardner 1985).

All analyses were performed within a Geographic Information System (GIS) environment (ArcGIS Pro) to ensure spatial consistency and correlation with geological features. These indices provide quantitative measures of active deformation and are widely used in tectonic geomorphology to identify zones of uplift, tilting, and fault-related topographic anomalies (Burbank and Anderson 2012; Keller and Pinter 2002).

The Stream Length-Gradient Index (SL), originally proposed by Hack (1973), was used to detect knickpoints and slope breaks along river profiles, which may reflect tectonic uplift or lithological contrasts. Anomalously high SL values, when correlated with mapped fault traces or lithological boundaries, often indicate neotectonic activity. The Hypsometric Integral (HI), calculated as the ratio of mean basin elevation to the elevation range, helps classify drainage basins as young (HI > 0.5), mature (HI ≈ 0.35–0.5), or old (HI < 0.35), providing insight into landscape evolution and potential tectonic rejuvenation (Strahler 1952; Burbank and Anderson 2012).

The Valley Floor Width to Valley Height Ratio (V*f*) is a critical parameter for assessing tectonic uplift. Low V*f* values suggest steep, V-shaped valleys associated with active tectonics, whereas higher values correspond to broad, U-shaped valleys formed under reduced tectonic influence (Hack 1957; Bull 1991). The Mountain Front Sinuosity (S*mf*) index, which compares the length of the mountain front to the straight-line distance along its base, provides a metric for evaluating the balance between erosion and uplift. Low S*mf* values (close to 1) indicate active, fault-controlled mountain fronts, whereas higher values suggest inactive or dominantly erosional fronts (Bull and McFadden 1977; Keller and Pinter 2002). Key S*mf* transects were selected along well-defined mountain fronts with minimal lithological contrast and clearly expressed fault traces, oriented perpendicular to the front to accurately capture its geomorphic expression.

The Basin Asymmetry Factor (A*f*), introduced by Hare and Gardner (1985), is sensitive to lateral tilting of drainage basins. Asymmetry in the drainage divide relative to the main stream direction may indicate tectonic tilting, especially when consistent across multiple sub-basins.

By integrating these indices with geological and structural observations, segments of the fault zones exhibiting differential uplift, recent deformation, or tectonic quiescence could be identified. This quantitative approach complements field-based analyses and aids in prioritizing areas for future paleoseismological investigations (Burbank and Anderson 2012; Keller and Pinter 2002).

The morphotectonic indices used in this study were calculated following standard formulations widely applied in tectonic geomorphology.

The hypsometric integral (HI), which characterizes the elevation distribution and erosional stage of a drainage basin, was calculated as:

$$HI = \frac{(Hmean - Hmin)}{(Hmax - Hmin)}$$

where Hmean, Hmax, and Hmin represent the mean,

maximum, and minimum elevations of each basin, respectively (Strahler 1952; Pike and Wilson 1971).

The stream length-slope index (SL), used to identify longitudinal channel steepness anomalies potentially related to tectonic or lithologic controls, was computed as:

$$SL = \left(\frac{\Delta H}{\Delta L}\right) L$$

where ΔH is the elevation difference along a channel segment, ΔL is the segment length, and L is the total upstream channel length from the drainage divide to the measurement point (Hack 1973). In this study, calculations were performed using a fixed segment length of 50 m consistent with the DEM resolution.

The valley floor width-height ratio (V*f*), which quantifies valley cross-sectional geometry and relative incision, was determined as:

$$Vf = \frac{2V_{fw}}{E_{ld} - E_{sc}} + E_{rd} - E_{sc}$$

where Vfw is the valley floor width, $E_{ld}$ and $E_{rd}$ are the elevations of the left and right valley divides, and $E_{sc}$ is the valley floor elevation (Bull and McFadden 1977).

Basin asymmetry was assessed using the asymmetry factor (A*f*):

$$Af = \frac{A_r}{A_t} \times 100$$

where Ar is the area to the right of the trunk stream (looking downstream) and At is the total basin area (Hare and Gardner 1985). Values greater or less than 50 indicate rightward or leftward tilting, respectively.

Mountain-front sinuosity (S*mf*), used to evaluate the degree of tectonic versus erosional control on mountain-front morphology, was calculated as:

$$Smf = \frac{L_{mf}}{L_s}$$

where Lmf is the actual length of the mountain front along its base and Ls is the straight-line length of the same front (Bull and McFadden 1977). Lower values close to 1 indicate straighter, structurally controlled fronts, whereas higher values reflect increased erosional modification. The 12.5 m resolution ALOS PALSAR DEM used in this study is appropriate for regional-scale morphotectonic analysis and for identifying first-order geomorphic features associated with long-term tectonic forcing. However, its vertical accuracy (approximately ±12.7 m) approaches the lower detection limit for subtle or low-amplitude Late Pleistocene–Holocene surface deformation. Consequently, small-offset scarps, minor vertical displacements, or short-lived surface expressions associated with low slip-rate fault activity may remain unresolved at this resolution. Accordingly, the absence of observable deformation in the DEM should not be interpreted as definitive proof of fault inactivity, but rather as the absence of deformation exceeding the detection threshold of the dataset. For this reason, DEM-based observations are interpreted in conjunction with field observations, stratigraphic relationships, and structural data to constrain the recent activity of the Savrun Fault.

### Integration of satellite imagery and geospatial data

High-resolution satellite imagery (Sentinel-2, ALOS PALSAR and Google Earth Pro) was utilized to map geomorphic features, lineaments, and surface expressions of faulting. Combined with field observations, satellite data facilitated the delineation of morphotectonic zones and drainage anomalies. Spatial overlays of tectonic indices and geological maps enabled a comparative analysis of structural features with morphometric evidence. By combining these methodologies, the study provides a comprehensive evaluation of the tectonic behavior of the Savrun fault system and its relation to basin evolution and seismic hazard.

## RESULTS

### GIS-Based Morphometric Analyses

Geographic Information Systems (GIS) play a significant role in fault-related studies by facilitating data acquisition, visualization, and spatial analysis. The location, orientation, and deformation characteristics of fault zones can be effectively assessed through GIS-based mapping and the use of digital elevation models (DEMs). In this study, a series of morphometric indices—Hypsometric Integral (HI) and hypsometric curve, Stream Length-Gradient Index (SL), Asymmetry Factor (A*f*), Valley Floor Width-to-Height Ratio (V*f*), and Mountain Front Sinuosity (S*mf*) were analyzed using ArcMap 10.8 and related toolboxes to evaluate the influence of tectonic processes on the morphology of the Savrun Fault zone.

### Hypsometric Integral (HI) and Curve

For hypsometric analysis, the area surrounding the Savrun Fault was divided into 10 sub-basins

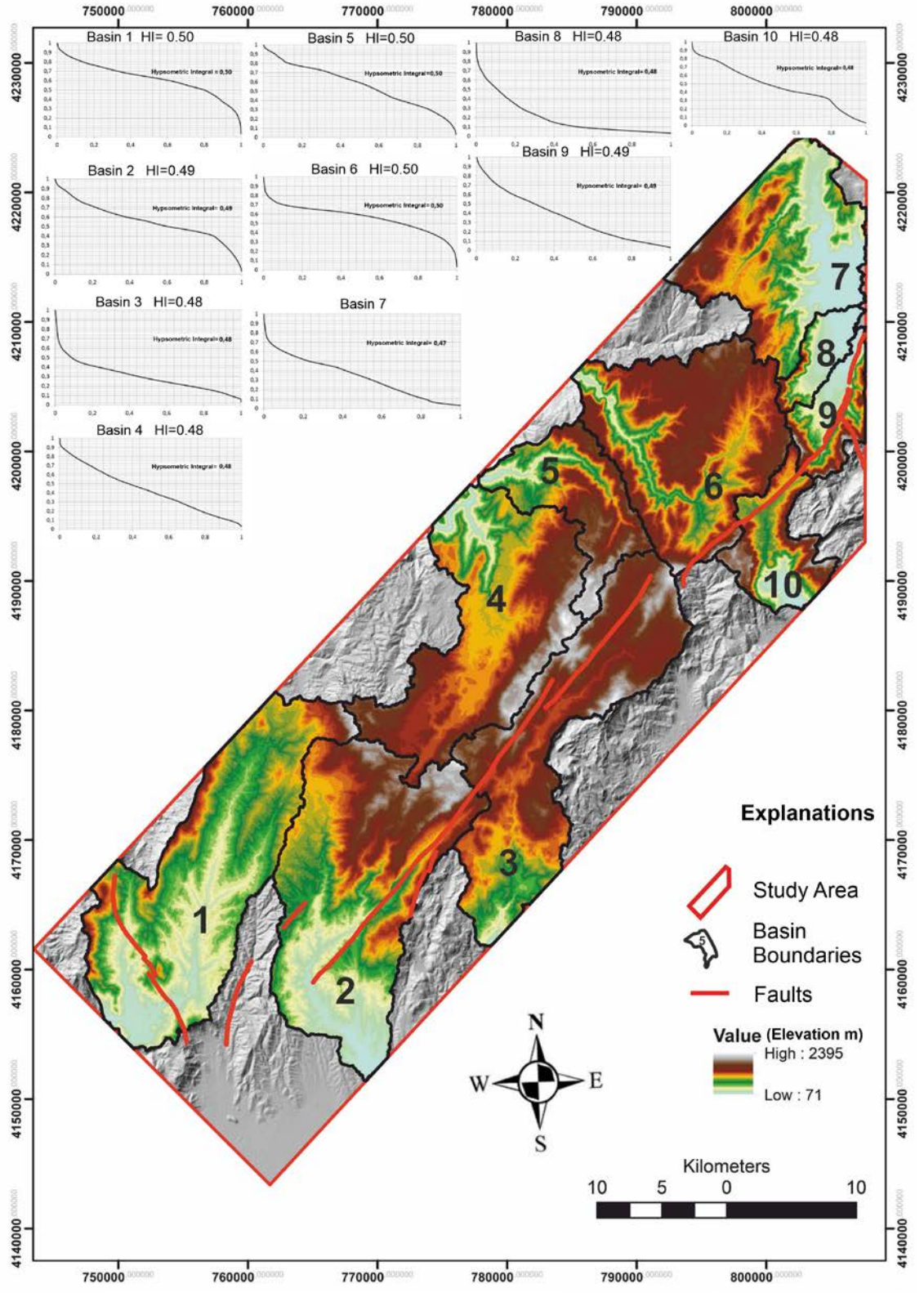


Fig. 4. Morphology and hypsometric analysis of the Savrun Fault. The main map shows the sub-basins delineated along the fault trace for Hypsometric Integral (HI) calculations. Sub-basin boundaries were defined using DEM-derived drainage networks. The upper-left inset displays the hypsometric curves for each sub-basin, illustrating relative stages of landscape evolution and potential tectonic influence along the fault.

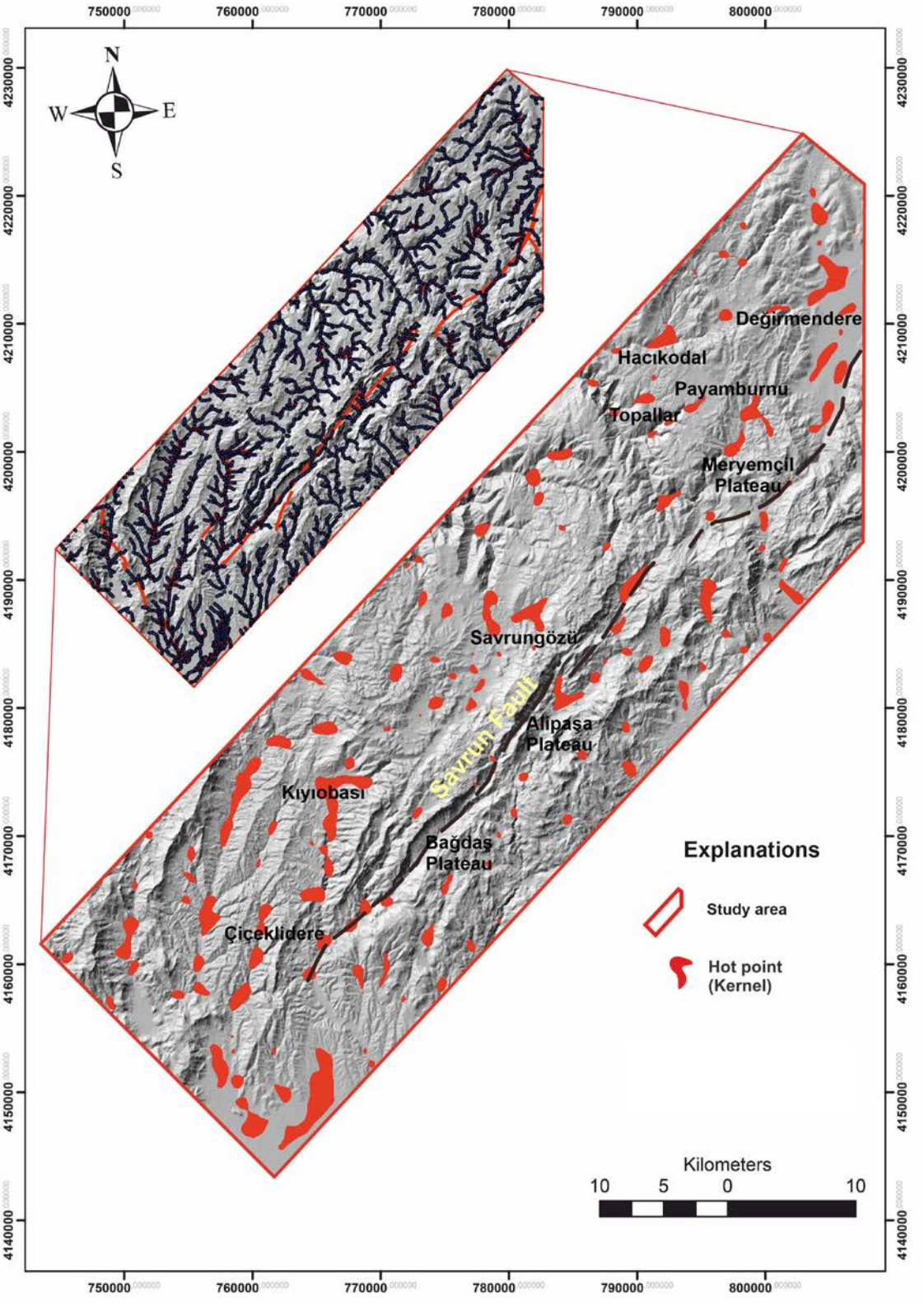


Fig. 5. Kernel density hotspot distribution of Stream Length-Gradient (SL) index values along the Savrun Fault. The inset map displays individual SL knickpoint measurement locations along the drainage network, plotted as blue points with black outlines; their dense clustering gives rise to a drainage-like linear pattern.

based on drainage systems. Sub-basins 2, 3, 6, 9, and 10 are located along the main fault trace, whereas the remaining basins are positioned adjacent to subsidiary or conjugate structural lineaments and zones of documented aftershock distribution (Text-fig. 4).

The calculated hypsometric integral (HI) values range between 0.47 and 0.50 across all sub-basins (Text-fig. 4). The corresponding hypsometric curves display generally smooth and moderately concave profiles with limited variation between basins. No pronounced asymmetry or abrupt inflection points are observed in the curve geometries. Basin morphologies are broadly comparable in terms of relief distribution and elevation-area relationships (Text-fig. 4).

### SL Index

Maps generated using the Slix Tool within ArcMap 10.8 (Text-fig. 5) display river networks, channel slope variations, calculated SL index values, and mapped fault traces. The SL index was calculated along the entire drainage network using a fixed stream segment length (dL) of 50 m, based on the 12.5 m DEM resolution and the spatial extent of the study area. The Stream Length-Slope Hot Spot and Clustering Analysis (SL-HCA) model of Troiani *et al.* (2017) was applied to identify statistically significant clusters of elevated SL values. In this context, the term "hot spot" denotes kernel density-based statistical clustering and does not represent any thermal or volcanic feature. Kernel density analysis shows that elevated SL values are distributed throughout the study area, with a localized concentration along the southern branch of the Savrun Fault extending through the Çiçeklidere-Esenli-Bağdaş plateau valley. Additional anomaly clusters are observed in the Topallar, Hacıkodal, Savrungözü, Kıyıobası and Payamburnu areas (Text-fig. 5).

Several anomaly zones spatially coincide with mapped landslide areas and steep slope sectors, particularly along the southeastern portion of the fault trace.

### V*f* index

The V*f* index is calculated as the ratio between valley floor width and the elevation difference of the valley sides and is commonly used to characterize valley morphology. Low V*f* values correspond to narrow valley floors with steep side slopes, whereas higher values indicate broader valley geometries.

To evaluate the geomorphic character of the principal valley systems along the Savrun Fault, 15 representative cross-sections were extracted and corresponding V*f* values were calculated (Text-figs 6, 7). Cross-sections were positioned along representative valley corridors morphologically associated with the fault zone and extracted perpendicular to valley axes; because the Savrun Fault commonly follows valleys or mountain fronts, some sections may appear oblique to the fault trace. The resulting valley profiles display considerable variation. Sections a, c, d, f–i and k–m exhibit relatively narrow valley floors with steep side slopes, while sections b, e, j and n display broader valley geometries. These morphological differences are spatially distributed along both the northern and southern branches of the fault trace. The profiles collectively show variability in valley width, slope angles, and cross-sectional symmetry (Text-figs 6, 7).

### A*f* Index

The Asymmetry Factor (A*f* index) is used to quantify the directional deviation of drainage basins. Values greater than 50 indicate rightward basin asymmetry, whereas values below 50 indicate leftward asymmetry. In this study, 12 sub-basins within and around the Savrun Fault zone were delineated from the drainage network and A*f* values were calculated for each basin (Text-fig. 8). Several of these basins are located slightly north and west of the mapped fault trace.

The calculated A*f* values show that, with the exception of sub-basin 9, all basins exhibit leftward asymmetry. Sub-basins 1, 5, 8, and 10 display the highest deviation values. The spatial distribution of asymmetric basins overlaps the northwestern sector of the study area where aftershock concentrations have been mapped (Text-fig. 8). Basin geometries collectively demonstrate variability in drainage orientation and asymmetry magnitude across the study area.

### S*mf* index

The S*mf* index (Mountain Front Sinuosity) is used to quantify the geometric irregularity of mountain fronts, where lower values correspond to straighter fronts and higher values indicate increased sinuosity. S*mf* analysis was conducted along 14 transects distributed across mountain fronts located along and around the Savrun Fault (Text-fig. 9). Mountain-front sinuosity (S*mf*) segments were systematically delineated along linear, fault-parallel mountain fronts that extend longitudinally along the Savrun Fault corridor. Segment selection focused primarily on continuous, well-defined geomorphic scarps and

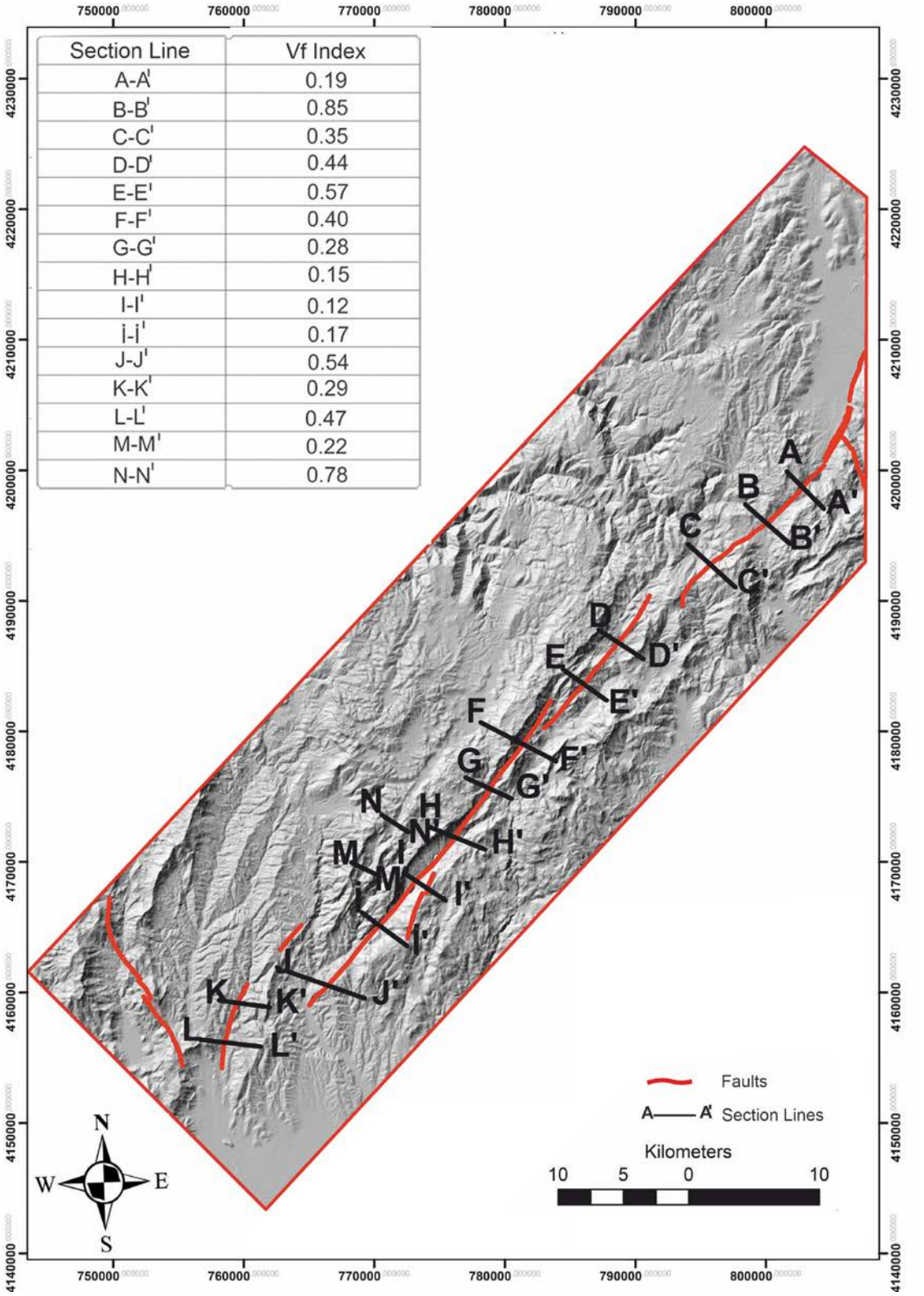


Fig. 6. Shaded relief map of the Savrun Fault zone showing the locations of the topographic cross-section lines used for the calculation of the Valley Floor Width-to-Height Ratio (V*f*). The upper-left inset presents the corresponding V*f* values derived from these cross-sections. The topographic cross-sections themselves are shown in Fig. 7.

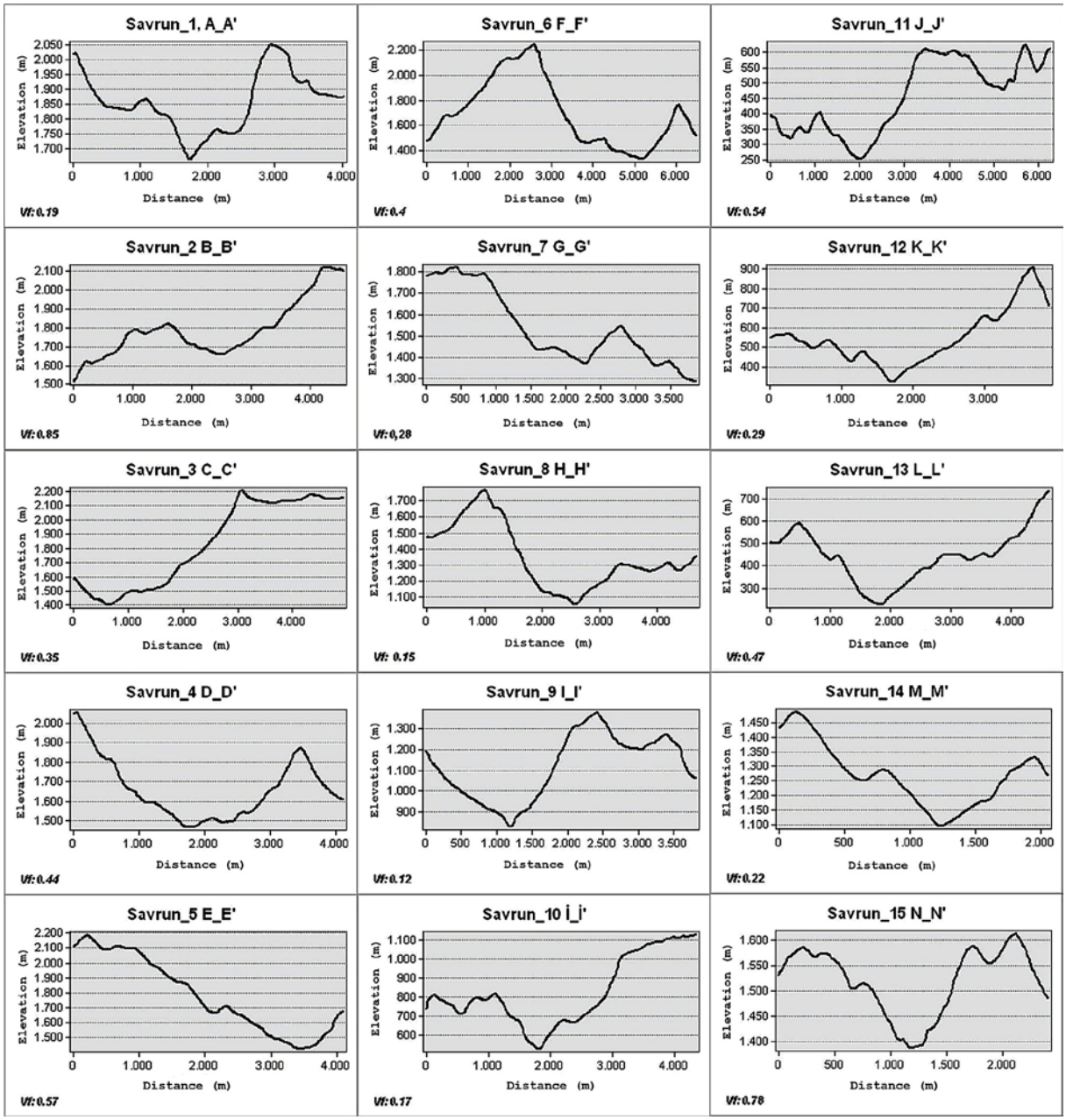


Fig. 7. Topographic cross-sections extracted along the Savrun Fault zone at the locations indicated in Fig. 6. These profiles illustrate the valley geometry used for the calculation of the Valley Floor Width-to-Height Ratio (V*f*) and provide detailed morphometric constraints for interpreting the geomorphic characteristics of the fault-related landscape.

range-front boundaries morphologically associated with the mapped fault trace. In addition, several segments were analyzed in nearby sectors displaying pronounced linear fronts and concentrated post-6 February 2023 aftershock activity, in order to evaluate whether localized neotectonic signals might be present outside the main fault strand (segments 4–7).

The calculated S*mf* values are presented in Textfig. 9 (inset). Transects 1, 2, 9, 10, 11, and 12 yield S*mf* values lower than 1.5 and display relatively straight mountain fronts. Transects 3, 5, and 7 show intermediate values between 1.5 and 1.7, whereas transects 4, 6, 8, 13, and 14 exhibit higher sinuosity values. Profiles 1 and 2 correspond to the southern and cen-

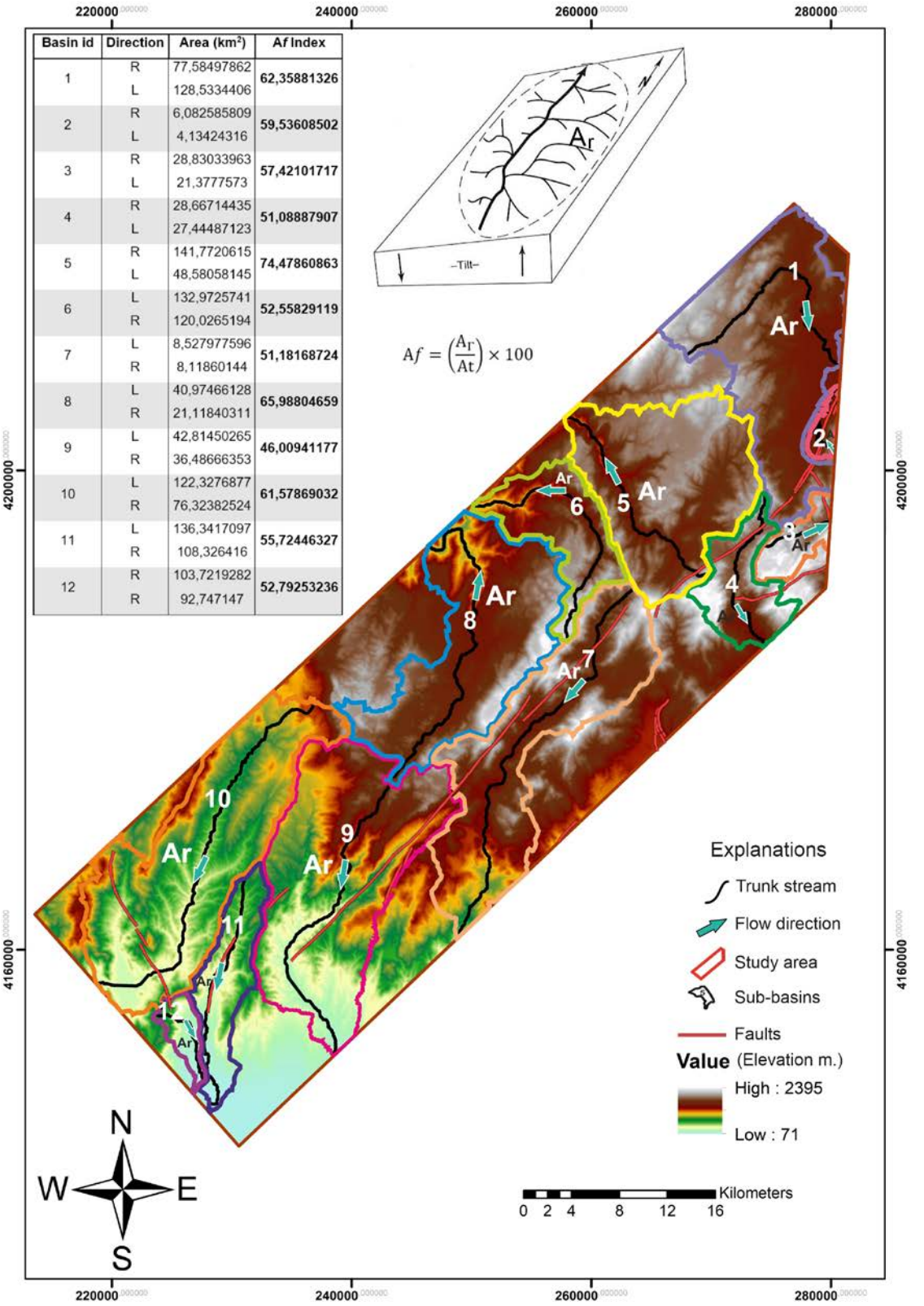


Fig. 8. A*f* index values calculated for sub-basins along the Savrun Fault, with basin numbers indicated on the map. The upper-left inset shows a table summarizing the calculated values, while the adjacent diagram presents the formula and method used for the A*f* index calculation.

| Id | Lmf | Ls | Smf=Lmf/Ls | Interpretation |
|---|---|---|---|---|
| 1 | 8,43145 | 7,646508 | 1,102653656 | Tectonically active |
| 2 | 10,060103 | 6,949156 | 1,447672638 | Tectonically active |
| 3 | 6,286921 | 3,976346 | 1,581079966 | Moderately active |
| 4 | 8,880892 | 4,47869 | 1,982921792 | Inactive / weakly active |
| 5 | 6,415761 | 3,842918 | 1,669502446 | Moderately active |
| 6 | 5,156395 | 2,725115 | 1,892175193 | Inactive / weakly active |
| 7 | 5,847592 | 3,623906 | 1,613615806 | Moderately active |
| 8 | 7,716837 | 3,120665 | 2,472818133 | Inactive / weakly active |
| 9 | 2,369512 | 1,916529 | 1,236355933 | Tectonically active |
| 10 | 6,963397 | 5,7915 | 1,202347751 | Tectonically active |
| 11 | 7,593597 | 5,594279 | 1,35738618 | Tectonically active |
| 12 | 8,893009 | 7,724819 | 1,15122555 | Tectonically active |
| 13 | 10,757301 | 4,50473 | 2,388001279 | Inactive / weakly active |
| 14 | 5,380816 | 3,011268 | 1,78689376 | Inactive / weakly active |

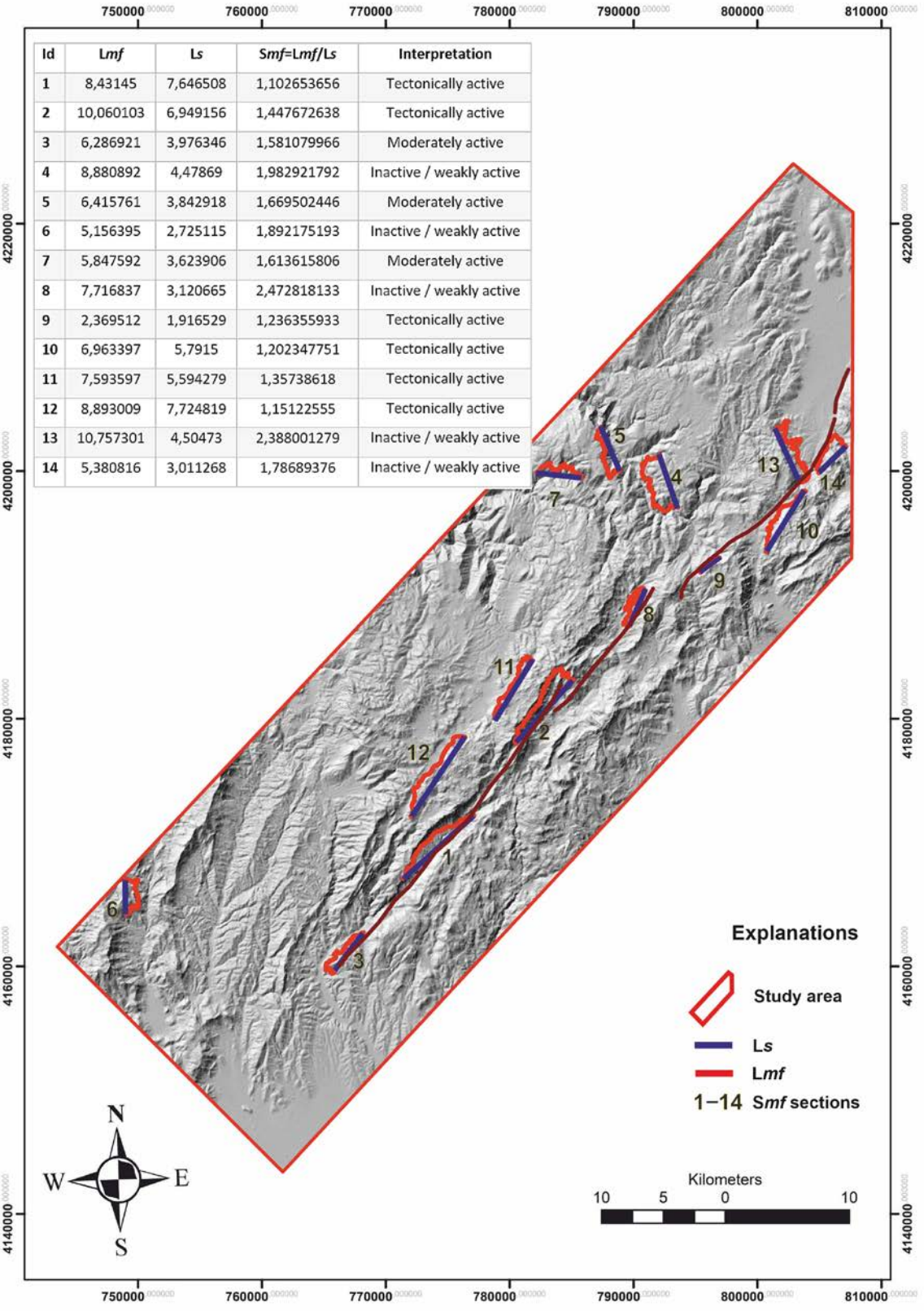


Fig. 9. Shaded relief morphometric map showing the locations and numbers of key S*mf* transects. The upper-left inset presents the calculated S*mf* values together with their corresponding interpretations of tectonic activity, classified as highly active, moderately active, or slightly active.

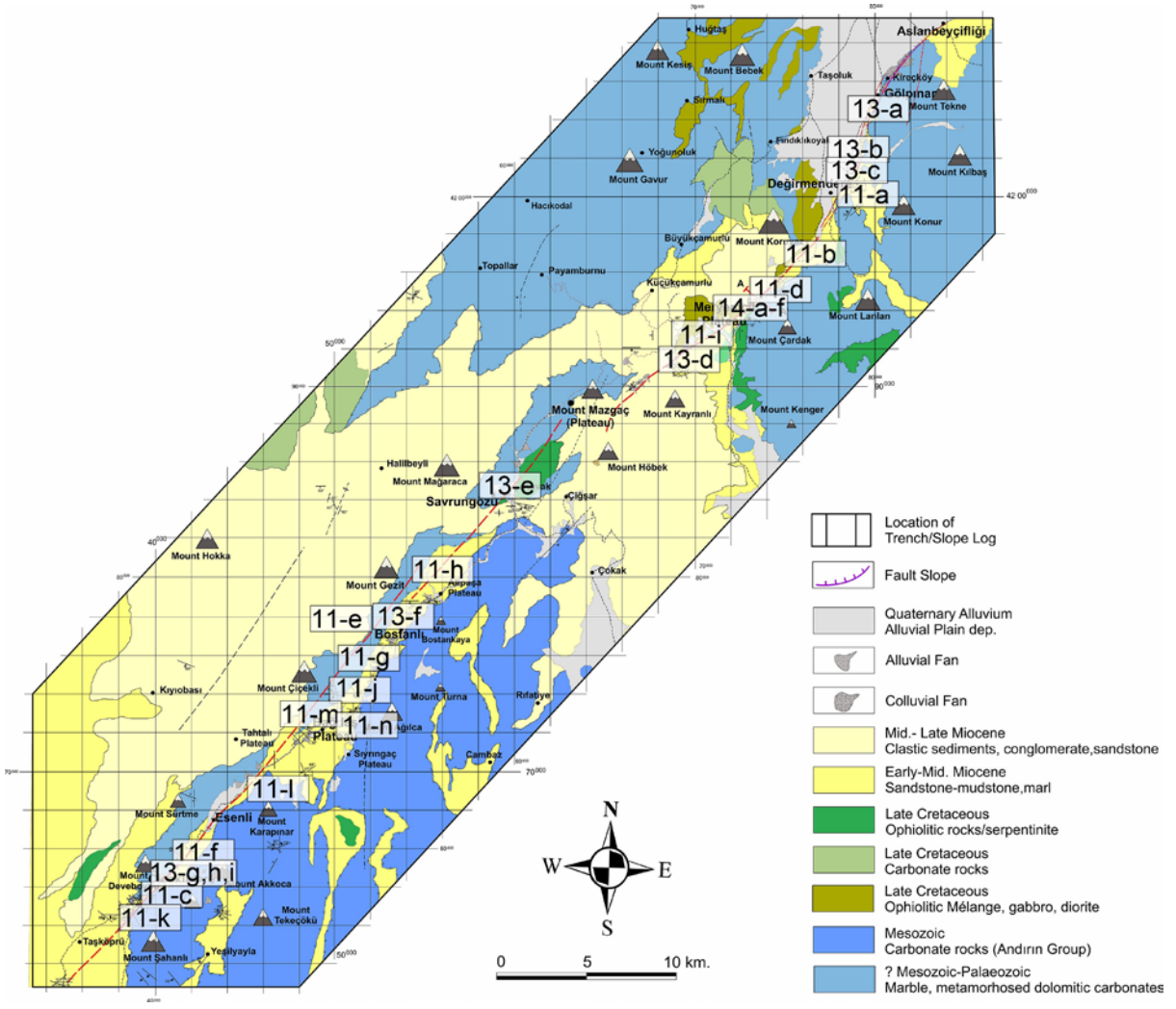


Fig. 10. Geological map of the Savrun Fault Zone illustrating the locations of field observation points and preliminary paleoseismological reconnaissance sites. Numbered labels correspond directly to the field photographs shown in Figs. 11–14.

tral segments of the Savrun Fault, profiles 9 and 10 represent the northern branch, and profiles 11 and 12 are located west of the mapped fault trace in an area characterized by frequent aftershock occurrence.

## Structural elements and kinematic analysis

Before presenting the structural measurements, the spatial distribution of the principal field observation sites and paleoseismological reconnaissance points is illustrated in Text-fig. 10. This map provides the geographic framework for the outcrop-scale structural data and cleaned slope exposures discussed below (Text-figs 10–13), allowing direct comparison between mapped fault traces and measured deformation structures.

This section presents detailed measurements and kinematic analyses of fault planes identified in stratigraphic units ranging from the Paleozoic to the Upper Miocene across the Savrun Fault zone (Text-fig. 11).

### Paleozoic units

A total of 11 fault-plane measurements were obtained from Paleozoic-aged carbonate and metamorphic units exposed in the northern and western sectors of the Savrun Fault (Text-fig. 12a). The majority of the measured faults display reverse fault kinematics.

Nine out of 11 fault planes exhibit reverse slip characteristics. Multiple generations of deformation structures are observed within these units, including

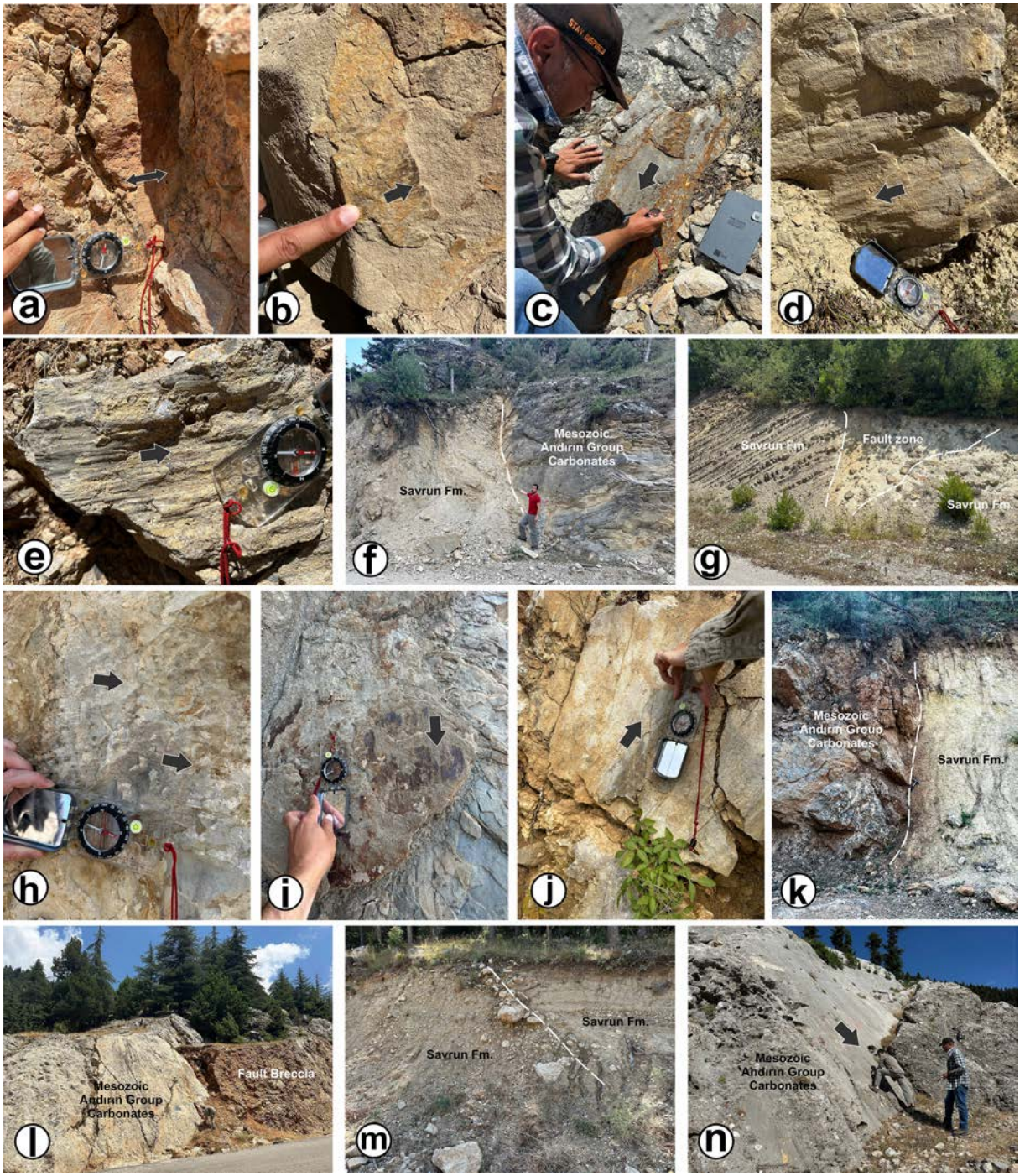


Fig. 11. Representative fault planes observed along different segments of the Savrun Fault. Measured kinematic indicators, including slickensides, lineations, and fault striations, are shown for each site, illustrating the orientation and sense of movement along the fault. Panels a, b, d, h, i, and j correspond to faults developed within the Early–Middle Miocene Savrun Formation; panel c is within the Mesozoic Andırın Group Unit (Carbonates), and panel e is within the Middle Miocene Gezitdağ Formation.

reverse faults, en-echelon structures, and folded features. The measured fault orientations and kinematic solutions are illustrated using stereographic projection diagrams in Text-fig. 12a.

## Mesozoic units

In the eastern segments of the Savrun Fault, five fault-plane measurements were collected from

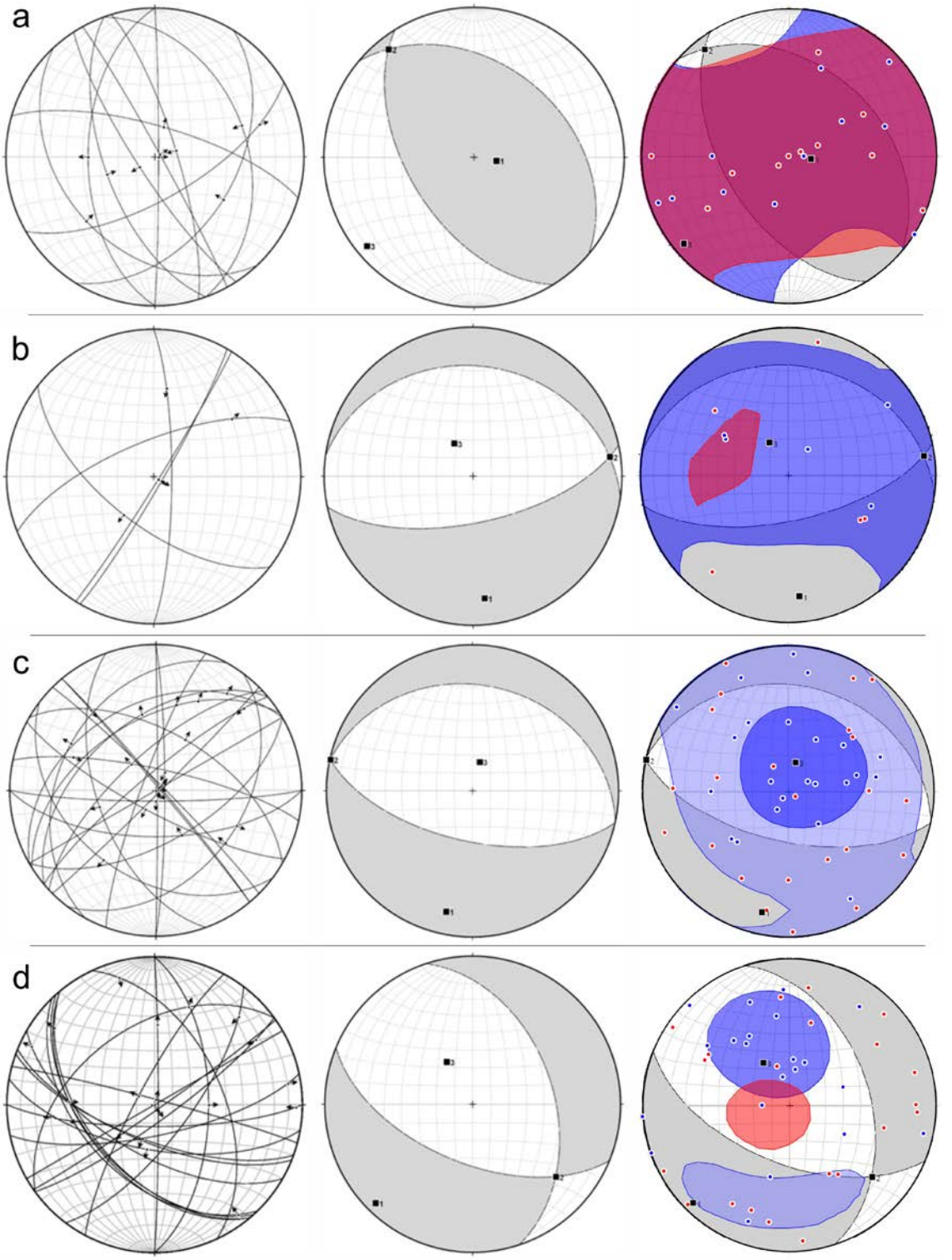


Fig. 12. Kinematic tensor analysis plots of fault-slip data collected from (a) Paleozoic, n = 11, (b) Mesozoic, n = 5, (c) Lower–Middle Miocene, n = 23, and (d) Middle–Upper Miocene units (n = 21) within the Savrun Fault zone and its surrounding area. In each panel, from left to right: stereographic projections of measured fault planes with associated slip-lineations, linked-Bingham kinematic analysis results illustrating principal stress orientations, and a combined display of scatter plots, contour diagrams, and lower-hemisphere fault-plane solutions. These diagrams summarize the orientation, sense of slip, and derived paleostress tensors for each stratigraphic unit, enabling temporal comparison of deformation patterns across the fault zone.

carbonate rocks of the Andırın Unit. The measured planes are moderately to steeply dipping and display well-developed slickenside lineations. The orientations and kinematic solutions are presented in stereonet projections in Text-fig. 12b.

Of the five measured fault planes, four display normal-slip kinematics and one exhibits reverse-slip indicators. The calculated kinematic solutions define a principal shortening direction oriented approximately NW-SE. The structures are spatially concentrated within the eastern fault segments and are restricted to Mesozoic bedrock exposures.

### Lower–Middle Miocene units

A total of 23 fault-plane measurements were collected from Lower–Middle Miocene clastic units exposed along the Savrun Fault valley beneath the Mesozoic thrust sheets of the Andırın Complex. The structural data are presented using stereonet projections and kinematic solutions in Text-fig. 12c. Of the measured fault planes, 18 exhibit normal-slip kinematics, 3 show oblique-slip components, and 2 display reverse-slip characteristics. The majority of the structures are moderately to steeply dipping and preserve well-developed slickenside lineations.

Kinematic analysis performed using the Linked Bingham method defines a dominant extensional stress configuration. The calculated T-axis is sub-horizontal with an azimuth of approximately 193°, whereas the P-axis is near-vertical. Reverse-slip faults are spatially concentrated in the western segment of the valley, while normal faults are more widely distributed throughout the study area.

### Middle–Upper Miocene units

A total of 21 fault-plane measurements were collected from Middle–Upper Miocene conglomeratic units exposed along the Savrun Fault valley and locally overlying the Andırın and Gezitdağ complexes. The structural data and corresponding stereonet projections are presented in Text-fig. 12d.

Of the measured fault planes, 15 display normal-slip kinematics, 3 exhibit reverse-slip components, and 3 show strike-slip characteristics. The majority of the faults are moderately to steeply dipping and preserve well-developed slickenside lineations. Kinematic solutions define a principal extension direction oriented approximately NE-SW to nearly N-S. Reverse and strike-slip structures are locally distributed among the normal faults within the conglomeratic sequence.

## Field observations and paleoseismic reconnaissance

The Savrun Fault connects with the E-W trending Çardak Fault near Aslanbeyçiftliği and Kireçköy, south of Göksun. At this junction, the fault bends approximately 65°–70° toward a NE orientation (N15°–20°E) and continues along the western flank of Teknedağı, bordering the Göksun Basin (Text-fig. 13a). Surface ruptures related to the February 6, 2023 earthquake sequence are observed along the Çardak Fault, where canal offsets are present; however, no coseismic deformation or surface rupture is observed along the mapped trace of the Savrun Fault.

Field observations along the Savrun Fault Zone indicate that the fault architecture is dominated by brittle deformation features, including fault breccias, gouge zones, and well-preserved slickenlined fault planes exposed in road cuts and stream sections. These structures document both strike-slip and dip-slip components and are consistently developed within consolidated Miocene and older units. The fault juxtaposes Paleozoic carbonates, flysch-type successions, and ophiolitic mélanges against Neogene clastic deposits, forming laterally continuous and well-exposed fault corridors suitable for structural analysis. In contrast, younger Quaternary colluvial and alluvial sediments generally overlie these units without observable displacement, suggesting that fault-related deformation did not propagate into the youngest deposits.

Southward toward Değirmendere, the fault trace is locally expressed by a subtle topographic break. Overlying Quaternary colluvial deposits show no visible displacement. Near the Değirmendere reservoir, the fault trends N30°–35°E, juxtaposing ophiolitic units against Lower–Middle Miocene clastics (Text-fig. 13b, c). The mountain front is characterized by a gentle slope rather than a sharp scarp. Cleaned exposures within young alluvial fans display continuous, undeformed bedding (Text-fig. 14). Fault planes are observable only within the underlying Miocene strata upslope.

Further south, along the NW slope of Kayranlı Mountain, Miocene fault structures are present in bedrock, whereas overlying colluvial fans remain undeformed. No displaced drainage channels or fault scarps are identified. Similar relationships are observed between the Savrungözü and Alipaşa plateaus, where the fault crosses Paleozoic carbonates and ophiolitic rocks without visible offsets in recent alluvium.

Along the Gezit Mountain front and Bağdaş Plateau, Middle–Upper Miocene deposits rest unconformably on the underlying Paleozoic basement car-

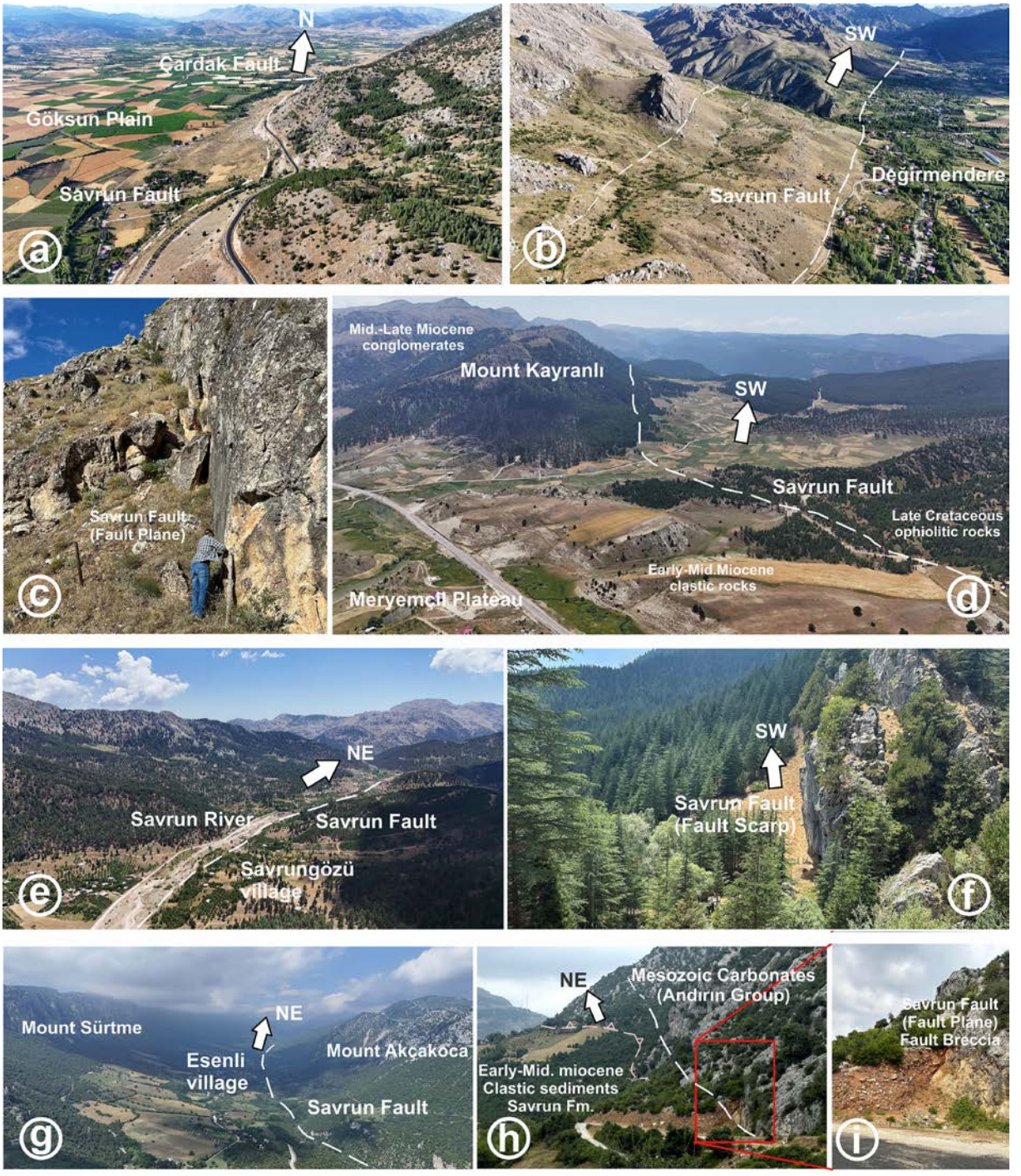


Fig. 13. Representative aerial and field photographs illustrating the morphological and structural characteristics (highlight fault-controlled linear valleys, scarps, offset geomorphic markers) along the Savrun Fault. a) Junction of the Çardak Fault and the Savrun Fault at the eastern margin of the Göksun Basin. The Çardak Fault, which generated the 2023 Elbistan earthquake (Mw 7.7), links with the Savrun Fault in this sector, highlighting the tectonic significance of their interaction; b) Extension of the Savrun Fault around Değirmendere village, c) Field view of the fault plane at the southern part of Değirmendere village, d) South of the Meryemçil plateau, the Savrun Fault extends with a slight bend toward the SW; e) Extend of the Savrun Fault at Savrungözü locality (no observable offset along the Savrun Stream), f) Field view of the Savrun Fault scarp around Bostanlı village; g) Extension of the southern strand of the Savrun Fault in the vicinity of Esenli village; h-i) Exposure of the Savrun Fault near Çiçeklidere, with the fault trace and associated breccia clearly visible on the right.

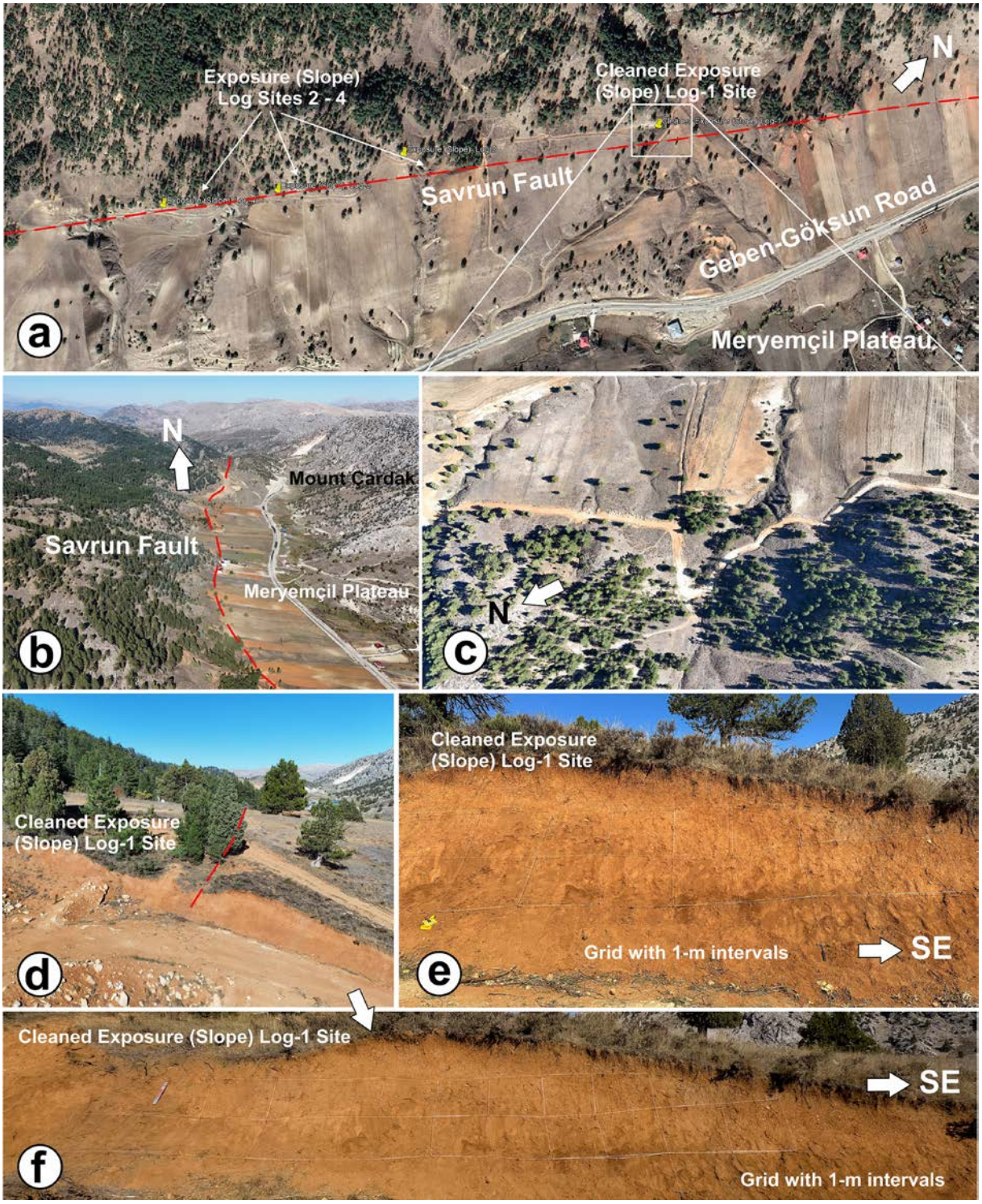


Fig. 14. Documentation of cleaned natural slope exposure logs investigated along the Savrun Fault near key Meryemçil Plateau area, south of Göksun. (a) Satellite image showing the location of the logged sites along the fault trace. (b) Drone view of the broader study area, illustrating the geomorphic setting of the exposures. (c) Close-up drone image of exposure Site 1, located within young alluvial deposits on a natural slope. (d) Oblique drone view highlighting the geometry and surface expression of Site 1. (e) Field photograph of Site 1 after cleaning and installation of a 1-m interval grid for systematic logging of the stratigraphy and structural features. (f) Panoramic view of Site 1 with the complete 1-m grid, documenting the entire logged exposure. The exposures collectively demonstrate that although the Savrun Fault trace lies beneath the young alluvial cover, these deposits show no evidence of deformation, indicating that the most recent surface faulting predates their deposition.

bonates and show no observable evidence of fault-related deformation. Large colluvial fans composed of carbonate and ophiolitic clasts show continuous stratification. In the southernmost sector near Şahanlı Mountain, the fault trace becomes morphologically indistinct and is represented mainly by high-angle lithologic contacts without clear geomorphic expression.

## DISCUSSION

### Field and stratigraphic constraints on Late Quaternary fault activity

Direct field and stratigraphic observations provide the most robust constraints on the recent activity of the Savrun Fault. Although regional compilations classify the fault as part of the active East Anatolian Fault Zone (Şaroğlu *et al.* 1992; Emre *et al.* 2013), and Gürboğa (2025) interpreted the Savrun Fault Zone as an active left-lateral strike-slip system, our detailed geological mapping and site-scale structural observations do not support evidence for Quaternary surface rupture.

Across the central and western segments of the fault trace, including the Gedikli, Tepecik, Karsavran and Karahamzalı areas, the fault remains geomorphically traceable but does not offset or disrupt the overlying Plio-Quaternary deposits. Instead, deformation is consistently confined to Lower–Middle Miocene clastic units and older bedrock. Young colluvial and alluvial sediments show continuous bedding, intact stratification, and no measurable displacement. These relationships are critical because undeformed Quaternary deposits directly overlying mapped fault strands represent a primary indicator that recent surface-rupturing events have not occurred.

Additional paleoseismological reconnaissance further supports this interpretation. Although no suitable trench sites were available due to the absence of well-preserved stratigraphy within Quaternary deposits, several cleaned slope exposures were examined in detail. The gridded exposure near the Meryemçil Plateau (Text-fig. 13), approximately 21 m wide and 1.8 m high, revealed bedding-parallel slip surfaces and minor deformation restricted to cemented Miocene conglomerates. Importantly, no evidence of colluvial wedges, growth strata, fissures, or displaced young sediments was observed (Text-fig. 13e, f). Such features would be expected if Late Pleistocene–Holocene rupture had occurred.

Furthermore, during the 6 February 2023 earthquake sequence, surface ruptures propagated along the adjacent Çardak Fault and displaced anthropogenic and geomorphic markers. However, no coseismic deformation extended onto the Savrun Fault. The absence of rupture during a major regional stress perturbation provides an independent, modern constraint consistent with limited present-day activity.

Taken together, the consistent absence of deformation in Late Pleistocene–Holocene deposits, combined with the restriction of faulting to older bedrock, strongly suggests that the most recent surface-rupturing phase along the Savrun Fault predates Quaternary sedimentation.

### Morphotectonic indices and geomorphic inheritance

Morphotectonic indices locally yield values that could be interpreted as indicative of tectonically active landscapes. However, when evaluated collectively and within their geological context, the results consistently suggest that the present morphology is controlled primarily by inherited Miocene topography and lithological contrasts rather than ongoing neotectonic uplift.

Hypsometric integral (HI) values show a narrow range of 0.47–0.50 across all analyzed sub-basins (Text-fig. 4), indicating uniformly mature basin geometries with limited relief differentiation. No systematic contrast is observed between basins located on or away from the fault trace, and the HI dataset therefore provides no evidence for localized uplift along the Savrun Fault.

Stream length-slope (SL) anomalies display a similarly non-systematic pattern. Elevated SL values are widely dispersed and do not consistently coincide with the mapped fault trace. Instead, clusters occur in sectors affected by steep slopes, landslides, and deep-seated gravitational slope deformation. The SL-HCA hot-spot clusters along the Çiçeklidere-Esenli-Bağdaş plateau valley correspond to inherited structural fabrics and lithological boundaries rather than demonstrable neotectonic offsets, indicating that channel steepening is primarily lithologically and structurally controlled.

Valley floor width-height ratios (V*f*) exhibit strong variability both on and off the fault trace. Narrow and broad valleys occur in comparable structural settings, suggesting that valley morphology reflects long-term incision history and lithologic contrasts rather than systematic fault-related uplift. In several cases, narrow valleys appear to preserve inherited Miocene relief and mimic morphologies typically associated with active tectonics.

A*f* and S*mf* indices likewise fail to show consistent fault-parallel trends. A*f* values mainly indicate broad regional tilting, whereas S*mf* values record a mixture of preserved straight fronts and more sinuous erosional fronts. Straight mountain fronts are not uniquely aligned with the Savrun Fault, further arguing against direct neotectonic control.

Similar morphometric behavior in inherited landscapes has been widely documented (Bull and McFadden 1977; Keller and Pinter 2002; Burbank and Anderson 2012; Silva *et al.* 2003; Demoulin 2011; Gutiérrez *et al.* 2015). When integrated with the field and structural evidence, the morphometric results are therefore best interpreted as reflecting geomorphic inheritance rather than active faulting.

## Structural record and tectonic phases of deformation

The structural dataset provides one of the most direct constraints on the timing of deformation along the Savrun Fault, as fault-plane kinematics preserved in bedrock record the mechanical history of the fault system independent of geomorphic interpretation. Measurements from lithologies of different ages reveal a polyphase deformation history in which the youngest clearly documented structures are Miocene in age, whereas younger deposits remain undeformed (Table 1).

Paleozoic and Mesozoic units yield predominantly contractional and locally mixed kinematics, consistent with regional compressional tectonics related to closure of the Neotethys and emplacement of thrust complexes (Text-fig. 11a, b). These structures clearly predate Neogene sedimentation and therefore provide only a regional tectonic background rather than evidence for recent fault activity.

In contrast, the Miocene succession preserves the most abundant and diagnostic structural record. Lower–Middle Miocene clastic units yielded 23 fault-plane measurements (Text-fig. 11c; Table 1), of which the majority exhibit normal or oblique-slip kinematics. Linked Bingham analysis defines a sub-horizontal T-axis and near-vertical P-axis, indicating a dominant extensional stress regime. These relationships are consistent with basin-scale extension and crustal thinning during Miocene sedimentation. Although a few reverse or oblique-slip structures occur locally, these are spatially restricted and interpreted as minor strain accommodation within the broader extensional framework.

Middle–Upper Miocene conglomerates show comparable behavior, with 21 additional measurements dominated by normal faulting and minor strike-slip components (Text-fig. 11d). The similarity of kinematics between Lower–Middle and Middle–Upper Miocene units indicates that extension persisted through much of the Miocene. Together, these two datasets demonstrate that the principal and youngest well-preserved deformation phase along the Savrun Fault is Miocene in age.

Crucially, no comparable fault planes, slickenside lineations, or offsets were identified within Plio-Quaternary or younger deposits across the study area. Neither brittle structures cutting unconsolidated sediments nor measurable displacements of young stratigraphic markers were observed. This absence is particularly significant because any Late Pleistocene–Holocene reactivation would be expected to produce clear deformation within these materials.

Accordingly, the structural evidence indicates that while the Savrun Fault preserves a well-developed record of Miocene deformation, there is no direct kinematic evidence for post-Miocene or neotectonic

Table 1. Summary of fault kinematics and inferred tectonic phases along the Savrun Fault.

| Lithological unit | Stratigraphic age | Observed fault kinematics | Inferred tectonic regime / phase | Implications for neotectonic activity |
|---|---|---|---|---|
| Paleozoic carbonate and metamorphic units | Paleozoic | Predominantly reverse faulting; minor strike-slip components | Late Cretaceous–Paleogene compression related to Tethyan closure | Inherited deformation; no relevance to Quaternary activity |
| Mesozoic carbonate units (Andırın Complex) | Mesozoic | Normal and reverse faulting; oblique-slip locally observed | Progressive compressional tectonics during Tethyan closure (Cretaceous–Miocene) | Pre-Neogene deformation, unrelated to neotectonic processes |
| Lower–Middle Miocene clastic units | Lower–Middle Miocene | Dominantly normal faulting with minor oblique and reverse components | Miocene extensional regime associated with crustal thinning | Major phase of Savrun Fault activity |
| Middle–Upper Miocene conglomerates | Middle–Upper Miocene | Normal faulting dominant; minor strike-slip and reverse faults | Continued Miocene extension with local stress reorganization | Late-stage Miocene deformation |
| Plio-Quaternary deposits | Plio-Quaternary | No fault planes, surface ruptures, or displaced strata observed | No documented tectonic regime | No evidence for neotectonic or Quaternary reactivation |

reactivation. The present morphology of the fault is therefore best interpreted as the inherited expression of earlier tectonic phases rather than the product of ongoing displacement.

**Seismic history and recent stress transfer**

Seismic observations provide an independent and contemporary constraint on the present-day behavior of the Savrun Fault. If the fault were actively accommodating regional strain, one would expect historical or instrumental seismicity to align spatially with its mapped trace or to show evidence of coseismic reactivation during major regional earthquakes. However, both historical records and modern seismicity patterns suggest otherwise.

Historical earthquake catalogues compiled by Soysal *et al.* (1981), Ambraseys (1988), Ambraseys and Jackson (1998), Tan *et al.* (2008), Demirtaş (2019), and Duman and Emre (2013) indicate that most documented events in the region occurred away from the Savrun Fault trace (Text-fig. 15a). Although several moderate earthquakes (M ≥4.0) have been recorded within the broader area since the early instrumental period, their epicenters do not define a clear linear distribution parallel to the fault. Instead, seismicity appears to cluster along neighboring lineaments and known active structures.

The February 6, 2023 Mw 7.6–7.7 earthquake sequence provides a particularly valuable natural test of fault behavior. This event produced several meters of left-lateral displacement along the adjacent Çardak Fault and generated an extensive aftershock sequence. Despite the close proximity of the Savrun Fault to the rupture termination of the Çardak Fault, no coseismic surface rupture, secondary faulting, or measurable displacement was observed along the Savrun Fault trace during field investigations. Aftershock epicenters are concentrated approximately 10–15 km west of the Savrun Fault (Text-fig. 15b, c), rather than along its mapped geometry.

Focal mechanism solutions of these aftershocks (Text-fig. 15b, c) indicate predominantly strike-slip and normal-faulting kinematics consistent with deformation localized on neighboring active structures. Importantly, the Savrun Fault itself does not host a comparable cluster of events.

Published Coulomb stress modeling by AFAD (2023) further clarifies this behavior. The ΔCFS patterns discussed here are based on the coseismic stress modelling results reported by AFAD (2023). These models show that post-seismic ΔCFS changes associated with the 2023 rupture were directed primarily westward and away from the Savrun Fault. In other words, the fault did not experience significant positive stress loading that would favor reactivation. The absence of a mechanical response, combined with the lack of observed surface rupture, indicates that the Savrun Fault did not participate dynamically in the regional stress redistribution.

When considered together with the absence of displaced Quaternary deposits and the structural evidence for predominantly Miocene deformation, the seismic record supports the interpretation that recent strain is preferentially accommodated by adjacent active faults rather than by the Savrun structure itself.

**Integrated interpretation**

When considered together, the independent datasets converge on a consistent interpretation. Field and stratigraphic observations show undeformed Late Pleistocene–Holocene deposits, morphometric indices lack systematic fault-parallel signals, and structural measurements indicate that the youngest well-constrained deformation phase is Miocene in age. Historical and instrumental seismicity, including the 2023 earthquake sequence, likewise shows no clear spatial or mechanical association with the Savrun Fault.

Gürboğa (2025) interpreted the Savrun Fault Zone as an active left-lateral strike-slip system based primarily on kinematic indicators observed in colluvial fan deposits and shallow sedimentary exposures. Our observations from the same general sectors, however, do not reveal stratigraphic discontinuities, displaced Quaternary deposits, or demonstrable surface ruptures that would indicate Late Pleistocene–Holocene movement. Instead, all measurable fault planes and slickenside lineations are confined to consolidated Miocene bedrock, and overlying Plio-Quaternary sediments remain undeformed (Text-figs 12, 13).

These differences likely reflect the contrast between localized geomorphic or morphologic interpretations and site-specific stratigraphic and kinematic constraints. While the prominent surface expression of the Savrun Fault may suggest recent activity at a regional scale, the combined field, structural, and morphometric evidence presented here indicates that the preserved deformation is predominantly Miocene in age. Accordingly, the Savrun Fault is interpreted as morphologically inherited rather than demonstrably neotectonically active.

Taken together, these lines of evidence indicate that the fault is morphologically prominent but presently quiescent, and that its surface expression most

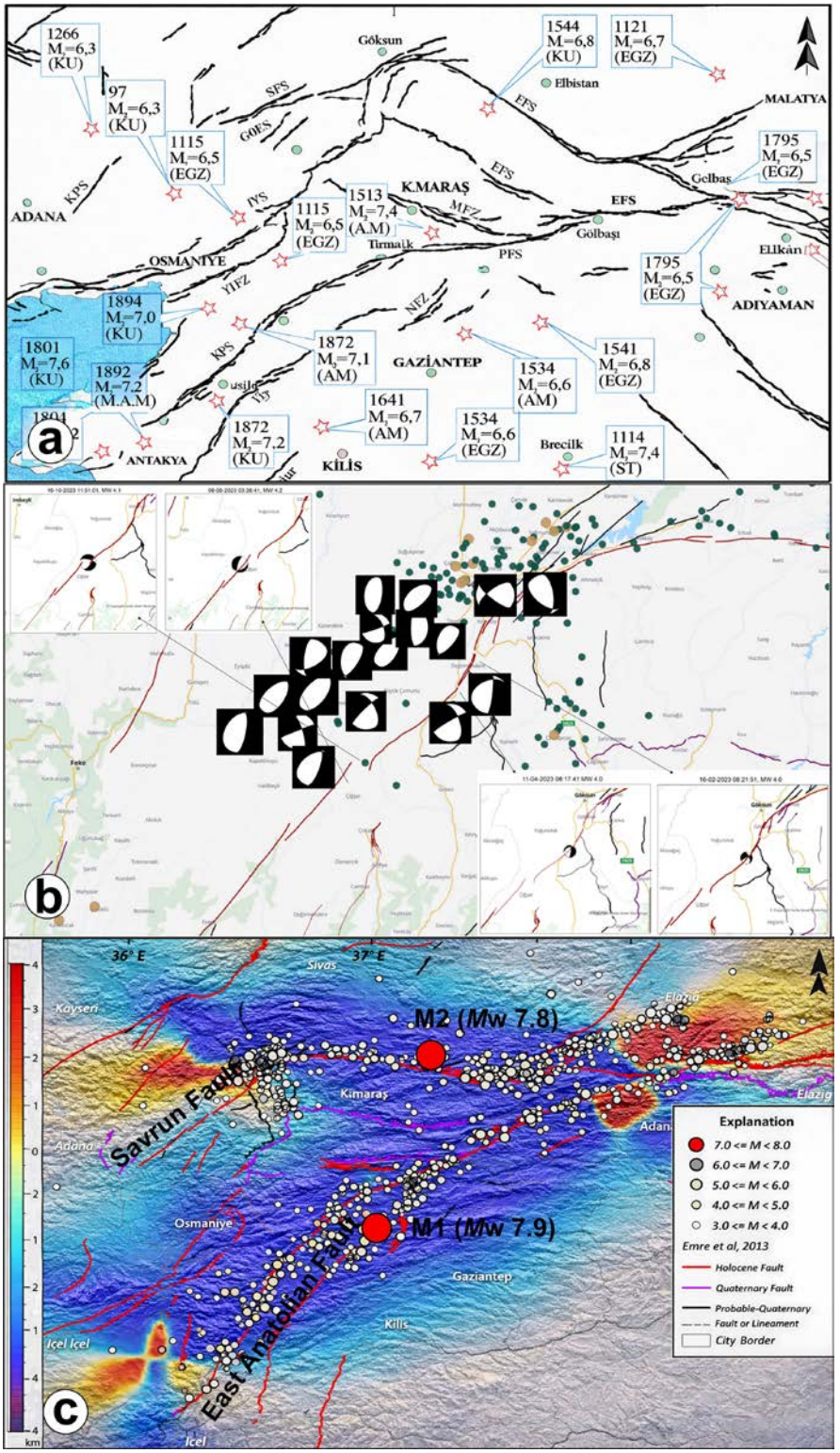


Fig. 15. Seismotectonic overview of southeastern Turkey. (A) Historical earthquake records in the region compiled and modified from Ambraseys (1988), Ambraseys and Jackson (1998), Tan *et al.* (2008), and Duman and Emre (2013), with abbreviations: ST, Shebalin and Tatevossian (1997); EG, Guidoboni *et al.* (1994); AM, Ambraseys (1988); AJ, Ambraseys and Jackson (1998). (B) Focal mechanism solutions of aftershocks along the fault following the February 2023 earthquakes, compiled from the AFAD earthquake catalog. (C) Regional Coulomb stress change (ΔCFS) distribution for the Mw 7.8 and Mw 7.7 mainshocks of the 2023 Kahramanmaraş earthquakes, based on the modelling results of AFAD (2023).

likely reflects preserved Miocene deformation rather than active Late Quaternary tectonics. This interpretation suggests that the Savrun Fault does not currently act as a significant active strand within the regional strain field.

## CONCLUSIONS

Integrated field observations, lithostratigraphic relationships, morphometric indices and GIS-based analyses consistently indicate that the Savrun Fault accommodated deformation during the Miocene. Well-developed fault planes and fracture systems are confined to Lower–Middle Miocene clastic and carbonate units, whereas Plio-Quaternary colluvial and alluvial deposits show no clear evidence of displacement. Although geomorphic indices such as S*mf*, SL, HI, A*f* and V*f* locally resemble signatures of tectonic uplift, these patterns are best explained by inherited Miocene topography and lithological contrasts rather than late-stage deformation.

The structural continuity of Miocene fabrics, the undisturbed character of younger sediments and the subdued expression of the fault toward its southern segments collectively suggest that motion along the Savrun Fault likely terminated during the Middle to Late Miocene. No stratigraphic discontinuities, colluvial wedges or surface ruptures were observed in Late Pleistocene to Holocene exposures, and the fault trace provides no suitable locations for paleoseismological trenching. Furthermore, despite the proximity of the Mw 7.6 Ekinözü rupture in 2023, the Savrun Fault showed no geomorphic or structural response to the regional stress redistribution.

Overall, the integrated structural, stratigraphic and morphotectonic evidence demonstrates that the Savrun Fault lacks indicators typically associated with post-Miocene or neotectonic reactivation. These results refine the Neogene tectonic evolution of the Kozan-Göksun corridor and contribute to a clearer understanding of fault architecture and inherited deformation patterns in southeastern Anatolia.

## Acknowledgements

This study was supported by Scientific and Technological Research Council of Türkiye (TUBITAK) under Grant number 123Y297. The authors thank TUBITAK for their support. The authors would like to thank the editor and anonymous reviewers for their constructive comments and insightful suggestions, which significantly improved the quality of this manuscript.

## REFERENCES

AFAD, 2023. 06 Şubat 2023 Kahramanmaraş (Pazarcık ve Elbistan) depremleri: saha çalışmaları ön değerlendirme raporu, 29 pp. Disaster and Emergency Management Presidency, Ankara.

AFAD, 2024a. Earthquake information website. Available at: https://deprem.afad.gov.tr/ (accessed 30 May 2024).

AFAD, 2024b. Online earthquake catalog. Available at: https://deprem.afad.gov.tr/event-catalog (accessed 30 September 2024).

AFAD, 2024c. Earthquake catalog of the Disaster and Emergency Management Presidency. Available at: https://deprem.afad.gov.tr/depremkatalogu (accessed 27 July 2024).

Akbaş, B., Akdeniz, N., Aksay, A., Altun, İ.E., Balcı, V., Bilginer, E., Bilgiç, T., Duru, M., Ercan, T., Gedik, İ., Günay, Y., Güven, İ.H., Hakyemez, H.Y., Konak, N., Papak, İ., Pehlivan, Ş., Sevin, M., Şenel, M., Tarhan, N., Turhan, N., Türkecan, A., Ulu, Ü., Uğuz, M.F., Yurtsever, A. *et al.* 2011. Geological map of Turkey at 1:1,250,000 scale. General Directorate of Mineral Research and Exploration (MTA), Ankara. [In Turkish]

Akıncı, A.C., Robertson, A.H.F. and Ünlügenç, U.C. 2016. Late Cretaceous–Cenozoic subduction-collision history of the Southern Neotethys: new evidence from the Çağlayancerit area, SE Turkey. *International Journal of Earth Sciences*, **105**, 315–337.

Akıncı, A.C. and Ünlügenç, U.C. 2021. Neogene tectonic evolution of the Misis-Andırın-Engizek Range: structural and sedimentary evidences from the Bulgurkaya sedimentary mélange. *Arabian Journal of Geosciences*, **14**, 655.

Akıncı, A.C. and Ünlügenç, U.C. 2023. Geological data, interpretations, and implications for Adana from the 6 February 2023 Kahramanmaraş earthquakes. Çukurova University *Journal of the Faculty of Engineering*, **38**, 553–569. [In Turkish with English abstract]

Aktaş, G. and Robertson, A.H.F. 1990. Tectonic evolution of the Tethys suture zone in SE Turkey: evidence from the petrology and geochemistry of Late Cretaceous and Middle Eocene extrusives. In: Malpas, J., Moores, E.M., Panayiotou, A. and Xenophontos, C. (Eds), Troodos 1987 Symposium, 311–328. Geological Survey Department; Nicosia.

Aktuğ, B., Özener, H., Doğru, A., Sabuncu, A., Turgut, B., Halıcıoğlu, K., Yılmaz, O. and Havazlı, E. 2016. Slip rates and seismic potential on the East Anatolian Fault System from an improved GPS velocity field. *Journal of Geodynamics*, **94–95**, 1–12.

Allmendinger, R.W., Aydin, A., Engelder, T. and Pollard, D.D. 1989. A Short Course on Quantitative Interpretation of Joints and Faults: Notes and Lectures, 59 pp. Geological Society of America; Boulder, Colorado.

Allmendinger, R.W., Cardozo, N. and Fisher, D.M. 2011. Struc-

tural Geology Algorithms: Vectors and Tensors, 304 pp. Cambridge University Press, Cambridge.

Allmendinger, R.W., Figueroa, D., Snyder, D., Beer, J., Mpodozis, C. and Isacks, B.L. 1990. Foreland shortening and crustal balancing in the Andes at 30°S latitude. *Tectonics*, **9**, 789–809.

Ambraseys, N.N. 1988. Engineering seismology. *Earthquake Engineering and Structural Dynamics*, **17**, 1–103.

Ayhan, A. 1983. Doğu Toroslar'da Kambro-Orodovisiyen Kayalarının Stratigrafisi ve Yayılımı. *Türkiye Jeoloji Kongresi Bülteni*, **4**, 17–20, Ankara.

Balkaya, M., Özden, S. and Akyüz, H.S. 2021. Morphometric and morphotectonic characteristics of the Sürgü and Çardak faults (East Anatolian Fault Zone). *Journal of Advanced Research in Natural and Applied Sciences*, **7**, 375–392. [In Turkish with English abstract]

Bedi, Y., Usta, D., Özkan, M.K., Beyazpirinç, M., Yıldız, H. and Yusufoğlu, H. 2005. Tectono-stratigraphic characteristics of the allochthonous units in the Eastern Taurus (Göksun-Sarız-Elbistan). Abstracts of the 58th Geological Congress of Turkey, 262–263. [In Turkish]

Blumenthal, M.M. 1952. New studies on the geography, stratigraphy and tectonics of the High Aladağ range, Taurus Mountains. *MTA Publications*, **6**, 136 pp. [In Turkish]

Bozkaya, Ö. and Yalçın, H. 1998. Diagenesis and very low-grade metamorphism related to sedimentary burial in Paleozoic rocks of the Eastern Taurus autochthon. *Bulletin of the Association of Petroleum Geologists of Turkey*, **10**, 35–54.

Bull, W.B. and McFadden, L.D. 1977. Tectonic geomorphology of mountain fronts. *Geological Society of America Bulletin*, **88**, 1475–1487.

Burbank, D.W. and Anderson, R.S. 2012. Tectonic Geomorphology. 2nd edition. Wiley-Blackwell; Chichester.

Burbank, D.W. and Anderson, R.S. 2013. Tectonic geomorphology. *Environmental and Engineering Geoscience*, **19**, 198–200.

Darbaş, G., Bayrak, F. and Gürel, A. 2021. Usability of the Yenicekale Formation exposure around Pazarcık (Kahramanmaraş) as cement raw material. *Bulletin of the Mineral Research and Exploration*, **166**, 53–69.

Dehbozorgi, M., Pourkermani, M., Arian, M., Matkan, A.A., Motamedi, H. and Hosseiniasl, A. 2010. Quantitative analysis of relative tectonic activity in the Sarvestan area, Central Zagros, Iran. *Geomorphology*, **121**, 329–341.

Demirtaş, R. 2019. Active faults of Turkey, seismicity, paleoseismology and future earthquake potential. 303 pp. Ankara. [In Turkish]

Demoulin, A. 2011. Basin and river profile morphometry: A new index with high potential for dating tectonic uplift. *Geomorphology*, **126**, 97–107.

Duman, T.Y. and Emre, Ö. 2013. The East Anatolian Fault: Geometry, segmentation and jog characteristics. *Geological Society, London, Special Publications*, **372**, 195–213.

El Hamdouni, R., Irigaray, C., Fernandez, T., Chacón, J. and Keller, E.A. 2008. Assessment of relative active tectonics, southwest border of Sierra Nevada (southern Spain). *Geomorphology*, **96**, 150–173.

Emre, Ö., Duman, T.Y., Özalp, S., Elmacı, H., Olgun, Ş. and Şaroğlu, F., 2013. Explanatory active fault map of Turkey, scale 1:1,250,000. General Directorate of Mineral Research and Exploration, Special Publication Series, No. 30,;Ankara.

Emre, Ö., Duman, T.Y., Özalp, S., Şaroğlu, F., Olgun, Ş., Elmacı, H. and Çan, T. 2016. Active fault database of Turkey. *Bulletin of Earthquake Engineering*, **14**, 1–47.

Esat, K. and Seyitoğlu, G. 2023. Preliminary field report on the 6 February 2023 Kahramanmaraş earthquakes, 4 pp. Unpublished report, Ankara. [In Turkish]

Goudie, A. (Ed.) 2004. Encyclopedia of Geomorphology, Vol. 2, 1200 pp. Routledge; London.

Guidoboni, E., Comastri, A. and Traina, G. 1994. Catalogue of ancient earthquakes in the Mediterranean area up to the 10th century, 505 pp. ING Roma-SGA; Bologna.

Gutiérrez, F. and Gutiérrez, M. 2016. Landforms of the Earth: An Illustrated Guide, 270 pp. Springer; Cham.

Güneyli, H. 1995. Geology and tectonics of the Horzum (Kozan-Adana) region. MSc Thesis, 129 pp. Çukurova University; Adana. [In Turkish]

Güneyli, H., Ünlügenç, U.C. and Demirkol, C. 1996. Stratigraphy of the Horzum Plateau and surroundings (Kozan/Adana). *Bulletin of the Geological Congress of Turkey*, **11**, 126–137. [In Turkish]

Gürboğa, Ş. 2025. Active tectonics and kinematic architecture of intraplate strike-slip fault: Savrun Fault Zone, SE Türkiye. *Journal of Asian Earth Sciences*, **281**, 106509.

Hack J.T. 1957. Studies of longitudinal stream profiles in Virginia and Maryland. *USGS Prof. Paper*, **259-B**, 45–97.

Hack, J.T. 1973. Stream profile analysis and stream gradient index. *Journal of Research of the U.S. Geological Survey*, **1**, 421–429.

Hall, R. 1976. Ophiolite emplacement and the evolution of the Taurus suture zone, southeastern Turkey. *Geological Society of America Bulletin*, **87**, 1078–1088.

Hare, P.W. and Gardner, T.W. 1985. Geomorphic indicators of vertical neotectonism along converging plate margins, Nicoya Peninsula, Costa Rica. In: Morisawa, M. and Hack, J.T. (Eds), Tectonic Geomorphology, 123–134. Proceedings of the 15th Annual Binghamton Geomorphology Symposium, Allen and Unwin; Boston.

Hempton, M.R., Dewey, J.F. and Şaroğlu, F. 1981. The East Anatolian Transform Fault: along-strike variations in geometry and behaviour. *EOS Transactions*, **62**, 393.

Herece, E. 2008. Atlas of the East Anatolian Fault. General Directorate of Mineral Research and Exploration, Special Publication 13, Ankara, 359 pp.

Hozatlıoğlu, D., Bozkaya, Ö., Yalçın, H. and Yılmaz, H. 2020.

Mineralogical characteristics of metamorphic massif units outcropping in Göksun, Afşin and Ekinözü (Kahramanmaraş) region. *Bulletin of the Mineral Research and Exploration*, **162**, 103–143.

Karig, D.E. and Kozlu, H. 1990. Late Palaeogene–Neogene evolution of the triple junction region near Maraş, south-central Turkey. *Journal of the Geological Society*, **147**, 1023–1034.

Keller, E.A. and Pinter, N. 1996. Active Tectonics: Earthquakes, Uplift, and Landscape, 359 pp. Prentice Hall,;New Jersey.

Keller, E.A. and Pinter, N. 2002. Active Tectonics: Earthquakes, Uplift, and Landscape. 2nd Edition, 362 pp. Prentice Hall,;Upper Saddle River.

Kelling, G., Davies, P. and Holroyd, J. 1987. Style, scale and significance of sand bodies in the Northern and Central Belts, southwest Southern Uplands. *Journal of the Geological Society*, **144**, 787–805.

Kelling, G., Egan, S.E., Gürbüz, K., Şafak, Ü., Ünlügenç, U.C. 2001. Oligo-Miocene basins of south-central Turkey: synthesis and appraisal, 24–28. Proceedings of the Fourth International Turkish Geology Symposium, Çukurova University; Adana.

Koç, A. 2005. Remote sensing study of the Sürgü Fault Zone (Malatya, Turkey). MSc Thesis, 90 pp. Ankara University; Ankara.

Koç, A. and Kaymakcı, N. 2013. Kinematics of the Sürgü Fault Zone (Malatya, Turkey): a remote sensing study. *Journal of Geodynamics*, **65**, 292–307.

Kozlu, H. 1997. Tectono-stratigraphy and development of Neogene basins (İskenderun, Misis-Andırın) in the Eastern Mediterranean region, 217 pp. Unpublished report; Ankara.

Kozlu, H., Sarıdaş, B. and Gül, M.A. 1979. Geology and petroleum potential of the Göksun-Saimbeyli region. TPAO Report No. 1389. Unpublished report; Ankara.

KRDAE 2023a. 6 February 2023 Ekinözü (Kahramanmaraş) earthquake bulletin, 6 pp. Kandilli Observatory and Earthquake Research Institute, Boğaziçi University; Istanbul.

KRDAE 2023b. Preliminary evaluation report of the 6 February Sofalaca-Şehitkamil-Gaziantep; Ekinözü-Kahramanmaraş and 20 February 2023 Hatay earthquakes, 25 pp. Kandilli Observatory and Earthquake Research Institute, Boğaziçi University; Istanbul.

Marrett, R.A. and Allmendinger, R.W. 1990. Kinematic analysis of fault-slip data. *Journal of Structural Geology*, **12**, 973–986.

Metin, S., Ayhan, A. and Papak, İ. 1986. Geology of the western part of the Eastern Taurus (GGD Turkey). *MTA Bulletin*, **107**, 1–13.

Muehlberger, R.W., andGordon, M.B. 1987. Observations on the complexity of the East Anatolian Fault, Turkey. *Journal of Structural Geology*, **9**, 899–903.

Nurlu, N., Parlak, O., Robertson, A. and Von Quadt, A. 2016. Implications of Late Cretaceous U-Pb zircon ages of granitic intrusions cutting ophiolitic and volcanogenic rocks in the Helete area (Kahramanmaraş, SE Turkey). *International Journal of Earth Sciences*, **105**, 283–314.

Özdoğan, M. and Şahbaz, A. 1993. Kozan (Adana Kuzeyi) Yöresi Miyosen Yaşlı Kırıntılı İstifin Stratigrafisi ve Dokusal Özellikleri, 46. Türkiye Jeoloji Kurultayı Bildiri Özleri, Ankara, 74.

Özdoğan, M. and Şahbaz, A. 1993. Stratigraphy and texture of Miocene clastic sequences north of Kozan (Adana). Abstracts of the 46th Geological Congress of Turkey, 74. [In Turkish]

Özgül, N. 1976. Some fundamental geological characteristics of the Taurus Mountains. *Bulletin of the Geological Society of Turkey*, **19**, 65–78. [In Turkish with English abstract]

Özgül, N. and Kozlu, H. 1993. Geology of the Kozan-Feke-Mansurlu area (Eastern Taurus). TPAO Report No. 3380, Ankara. [Unpublished]

Özgül, N. and Kozlu, H. 2002. Stratigraphy and structural position of the Kozan-Feke region (Eastern Taurus): New findings. *Bulletin of the Association of Petroleum Geologists of Turkey*, **14** (1), 1–36.

Özgül, N., Metin, S. and Dean, B.T. 1972. Lower Paleozoic stratigraphy and fauna around Tufanbeyli (Adana). *MTA Bulletin*, **76**, 9–16.

Pampal, S. 1983. Stratigraphic and tectonic characteristics of the Kadirli-Kozan-Feke (Adana) and Çokak (Kahramanmaraş) region. PhD Thesis, Selçuk University, Konya, 133 pp.

Pampal, S. 1984. Stratigraphy and tectonic characteristics of the Kadirli-Kozan-Feke region. Selçuk University Publications, Konya. [In Turkish]

Pampal, S. 1986. Geology of the Taşköprü (Kadirli)-Akçaluşağı-Zincirlikuyu (Kozan) region west of the Savrun Fault. *Gazi University Engineering Faculty Journal*, **1**, 65–100. [In Turkish]

Pampal, S. and Kurtman, F. 1983. New data on the Neo-Tethys rifting in the Eastern Taurus Region. In: Tekeli, O., Göncüoğlu, M.C. (Eds), *Geology of the Taurus Belt*, 217–222. MTA; Ankara.

Pike, R.J. and Wilson, S.E. 1971. Elevation-relief ratio, hypsometric integral, and geomorphic area-altitude analysis. *Geological Society of America Bulletin*, **82**, 1079–1084.

Robertson, A.H.F. 1998. Mesozoic–Tertiary tectonic evolution of the easternmost Mediterranean: integration of marine and land evidence. *Proceedings of the Ocean Drilling Program, Scientific Results*, **160**, 723–782.

Robertson, A.H.F. 2000. Mesozoic–Tertiary tectonic-sedimentary evolution of a South Tethyan oceanic basin and its margins in southern Turkey. In: Bozkurt, E., Winchester, J.A., Piper, J.D.A. (Eds), Tectonics and Magmatism in Turkey and the Surrounding Area, *Geological Society of London Special Publications*, **173**, 97–138.

Robertson, A.H.F., Ünlügenç, U.C., İnan, N., Taslı, K. 2004. The Misis-Andırın complex: a Mid-Tertiary mélange relat-

ed to late-stage subduction of the Southern Neotethys in S Turkey. *Journal of Asian Earth Sciences*, **22**, 413–453.

Rockwell, T.K., Keller, E.A. and Johnson, D.L. 1984. Tectonic geomorphology of alluvial fans and mountain fronts near Ventura, California. In: Morisawa, M. (Ed.), Tectonic Geomorphology, 183–207. John Wiley & Sons (Wiley-Blackwell); Chichester.

Rotstein, Y. and Ben-Avraham, Z. 1985. Accretionary processes at subduction zones in the eastern Mediterranean. *Tectonophysics*, **112**, 551–571.

Schiettecatte, J.P. 1971. Geology of the Misis Mountains. In: Campbell, M. (Ed.), Geology and History of Turkey, 305–312. Petroleum Exploration Society; London.

Selim, H.H., Tüysüz, O., Karakaş, A. and Taş, K.Ö. 2013. Morphotectonic evidence from the southern branch of the North Anatolian Fault and basins of the South Marmara sub-region (NW Turkey). *Quaternary International*, **292**, 176–192.

Silva, P.G., Goy, J.L., Zazo, C. and Bardají, T. 2003. Fault-generated mountain fronts in southeast Spain: Geomorphologic assessment of tectonic and seismic activity. *Geomorphology*, **50**, 203–225.

Soysal, H., Sipahioğlu, S., Kolçak, D. and Altınok, Y. 1981. Historical earthquake catalogue of Turkey and surroundings, 86 pp. TÜBITAK Project TBAG-341; Istanbul.

Strahler, A.N. 1952. Hypsometric (area–altitude) analysis of erosional topography. *Geological Society of America Bulletin*, **63**, 1117–1142.

Sunkar, M., Günek, H. and Canpolat, C. 2008. Geomorphology of Kurucaova and its surroundings (Malatya). *Firat University Journal of Social Sciences*, **18**, 1–22.

Şaroğlu, F., Emre, Ö. and Kuşçu, İ. 1992. The East Anatolian Fault Zone of Turkey. *Annales Tectonicae*, **6**, 99–125.

Şengör, A.M.C. and Yılmaz, Y. 1981. Tethyan evolution of Turkey: A plate tectonic approach. *Tectonophysics*, **75**, 181–241.

Tan, O.M., Tapırdamaz, C. and Yörük, A. 2008. Earthquake catalogues for Turkey. *Turkish Journal of Earth Sciences*, **17**, 405–418.

Troiani, F., Piacentini, D., Della Seta, M. and Galve, J.P. 2017. Stream length-gradient hotspot and cluster analysis (SL-HCA) for fine interpretation of knickzones on longitudinal profiles. *Catena*, **156**, 30–41.

Tutkun, S.Z. 1989. Tectonic characteristics of the Saimbeyli (Adana) region. *Journal of Geological Engineering*, **34**, 57–63. [In Turkish]

Usta, D., Şenel, M., Metin, Y., Bedi, Y., Vergili, Ö., Usta, M., Balcı, V., Kuru, K., Tok, T., Özkan, M.K. and Kop, A. 2004. Geological characteristics of structural units between Kozan-Tufanbeyli (Adana). Abstracts of the 57th Geological Congress of Turkey, 275–276. MTA; Ankara.

Usta, D., Usta, M., Balcı, V. and Kop, A. 2013. Geology and metallogeny of the Kozan–Feke region (Eastern Taurus), 272 pp. MTA Compilation Report 11635; Ankara.

Ünlügenç, U.C. 1993. Controls on Cenozoic sedimentation in the Adana Basin, Southern Turkey, 228 pp. PhD Thesis, Keele University; Keele.

Ünlügenç, U.C., Akıncı, A.C. and Güneyli, H. 2011. Tectonic elements of the Çukurova Basin Complex. ATAG 15 Abstracts, 6. Çukurova University; Adana.

Ünlügenç, U.C. and Akıncı, A.C. 2018. Geodynamical evolution of the Misis Structural High, Ceyhan (Adana), Southern Turkey. 9th International Symposium on Eastern Mediterranean Geology, 374–379. Akdeniz University; Antalya.

Ünlügenç, U.C. and Akıncı, A.C. 2019. Determination of geometries of active faults in the Çukurova region, 35 pp. Çukurova University Research Project FBA-2017-8064; Adana.

Ünlügenç, U.C., Akıncı, A.C. 2024. Seismicity of Adana Province and faults capable of generating earthquakes. *Yerbilimleri (Geosound)*, **59**, 69–93.

Westaway, R. 2003. Kinematics of the Middle East and Eastern Mediterranean updated. *Turkish Journal of Earth Sciences*, **12**, 5–46.

Westaway, R. 2004. Kinematic consistency between the Dead Sea Fault Zone and Neogene–Quaternary left-lateral faulting in SE Turkey. *Tectonophysics*, **391**, 203–237.

Yılmaz, Y. and Gürer, Ö.F. 1996. Geology and evolution of the Misis-Andırın Belt around Andırın (Kahramanmaraş). *Turkish Journal of Earth Sciences*, **5**, 39–55.

Yılmaz, Y., Gürpınar, Ö.F., Gül, M.A., Kozlu, H., Yıldırım, M. *et al.* 1985. Geology of the northern Maraş region (Engizek-Berit-Nurhak-Binboğa-Andırın Mountains). TPAO Report No. 2028, 161 pp. [Unpublished]

*Manuscript submitted: 15th January 2026*
*Revised version accepted: 17th March 2026*